

A posteriori error estimates for combined finite volume–finite element discretizations of reactive transport equations on nonmatching grids*

Danielle Hilhorst¹, and Martin Vohralík²

¹ Laboratoire de Mathématiques, Analyse Numérique et EDP, Université de Paris-Sud et CNRS, Bât. 425, 91 405 Orsay, France. danielle.hilhorst@math.u-psud.fr

² UPMC Univ. Paris 06, UMR 7598, Laboratoire Jacques-Louis Lions, 75005, Paris, France & CNRS, UMR 7598, Laboratoire Jacques-Louis Lions, 75005, Paris, France. vohralik@ann.jussieu.fr

Abstract

We derive in this paper guaranteed and fully computable a posteriori error estimates for vertex-centered finite-volume-type discretizations of transient linear convection–diffusion–reaction equations. Our estimates enable actual control of the error measured either in the energy norm or in the energy norm augmented by a dual norm of the skew-symmetric part of the differential operator. Lower bounds, global-in-space but local-in-time, are also derived. These lower bounds are fully robust with respect to convection or reaction dominance and the final simulation time in the augmented norm setting. On the basis of the derived estimates, we propose an adaptive algorithm which enables to automatically achieve a user-given relative precision. This algorithm also leads to efficient calculations as it balances the time and space error contributions. As an example, we apply our estimates to the combined finite volume–finite element scheme, including such features as use of mass lumping for the time evolution or reaction terms, of upwind weighting for the convection term, and discretization on nonmatching meshes possibly containing nonconvex and non-star-shaped elements. A collection of numerical experiments illustrates the efficiency of our estimates and the use of the space–time adaptive algorithm.

Key words: transient convection–diffusion–reaction equation, finite volume method, finite element method, convection dominance, inhomogeneous and anisotropic diffusion, nonmatching grids, a posteriori error estimates, guaranteed upper bound, adaptive mesh refinement

AMS subject classifications: 65M15, 65M60, 76M12, 76S05

*This work was supported by the GNR MoMaS (PACEN/CNRS, ANDRA, BRGM, CEA, EdF, IRSN), France.

1 Introduction

We consider in this paper the time-dependent linear convection–diffusion–reaction problem

$$u_t - \nabla \cdot (\mathbf{S} \nabla u) + \nabla \cdot (u \mathbf{v}) + ru = f \quad \text{in } \Omega \times (0, T), \quad (1.1a)$$

$$u(\cdot, 0) = u_0 \quad \text{in } \Omega, \quad (1.1b)$$

$$u = 0 \quad \text{on } \partial\Omega \times (0, T), \quad (1.1c)$$

where \mathbf{S} is in general an inhomogeneous and anisotropic (nonconstant full-matrix) diffusion–dispersion tensor, \mathbf{v} is a (dominating) velocity field, r is a reaction function, f is a source term, u_0 prescribes the initial condition, $\Omega \subset \mathbb{R}^d$, $d = 2, 3$, is a polygonal (polyhedral for $d = 3$) domain (open, bounded, and connected set), and $(0, T)$ is a time interval. Our purpose is to derive a posteriori error estimates for conforming locally conservative discretizations of problem (1.1a)–(1.1c). A particular attention will be paid to the combined finite volume–finite element scheme [13].

One of the first works on a posteriori error estimates for finite element discretizations of steady convection–diffusion–reaction problems are those of Angermann [2] and of Eriksson and Johnson [9]. In these works, the overestimation factor depends unfavorably on the ratio between convection and diffusion. Estimates with semi-robust lower bounds in the energy norm and estimates with robust lower bounds in the energy norm augmented by the dual norm of the convective derivative were then derived by Verfürth respectively in [23] and [26]. The robustness result has been extended to the unsteady case by Verfürth in [25]. Recently, attention has also been paid to vertex-centered finite volume methods. Let us mention, in the steady convection–diffusion–reaction case and energy norm setting, Lazarov and Tomov [17], Carstensen et al. [6], Nicaise [18], [30], and Ju et al. [16]. Fewer results are known in the unsteady case. L^1 -norm estimates for nonlinear problems are derived by Ohlberger [19], whereas the energy norm setting has been pursued in, e.g., Felcman and Kubera [15] or Amaziane et al. [1]. Typically, the estimate only gives the error upper bound up to an undetermined constant, so that the actual error control is not possible, and the lower bound proof is not given or states a non-robust result.

The present paper aims at enriching the known results for vertex-centered finite-volume-type methods in several directions. Firstly, we derive estimates which are guaranteed (not featuring any undetermined constants) and fully and easily computable. We achieve this by introducing $\mathbf{H}(\text{div}, \Omega)$ -conforming locally conservative diffusive and convective flux reconstructions, following [29, 31, 10, 11]. Consequently, the estimates allow for actual error control in unsteady convection–diffusion–reaction problems. Secondly, we propose a space–time adaptive algorithm which equilibrates properly the time and space contributions in the sense that they are in actual balance, not weighted by any undetermined quantities. Moreover, this algorithm is proposed to guarantee a user-given relative precision in the simulation. Thirdly, following [25], we also prove a lower error bound. Fourthly, our results are valid for a larger family of conforming locally conservative discretizations, in the framework of the so-called combined finite volume–finite element method, cf. Feistauer et al. [14] and the references therein. Consequently, the analysis includes such features as use of mass lumping for the time evolution or reaction terms or use of upwind weighting for the convection term. Lastly, we also treat the case of very general non-matching meshes possibly containing nonconvex and non-star-shaped elements; convergence analysis of the combined finite volume–finite element method on such meshes (for degenerate parabolic convection–diffusion–reaction problems) was carried out in [13].

The paper is organized as follows: in Section 2, the continuous problem is described. Section 3 collects the notation of the discrete setting and introduces the combined finite volume–finite element scheme. In Sections 4 and 5, the a posteriori error estimate and its efficiency is respectively stated and proved. Finally, an adaptive algorithm is presented in Section 6 and numerical experiments in Section 7. Some conclusions are drawn in Section 8.

2 The continuous setting

We state in this section our assumptions on the data and define a weak solution of problem (1.1a)–(1.1c).

2.1 Assumptions on the data

Let the time interval $(0, T]$ be split such that $0 = t_0 < \dots < t_n < \dots < t_N = T$ and define $\tau_n := t_n - t_{n-1}$, $n \in \{1, \dots, N\}$. On each time interval $(t_{n-1}, t_n]$, $n \in \{1, \dots, N\}$, consider a partition \mathcal{D}_h^n of Ω into closed polygons such that $\bar{\Omega} = \bigcup_{D \in \mathcal{D}_h^n} D$ and such that the intersection of the interiors of two different polygons is empty. Also set $Q_T := \Omega \times (0, T)$.

We suppose that the data of problem (1.1a)–(1.1c) satisfy:

Assumption (A) (Data)

(A1) $\mathbf{S}_{ij} \in L^\infty(Q_T)$, $1 \leq i, j \leq d$, is a symmetric, bounded, and uniformly positive definite tensor such that for all $n \in \{1, \dots, N\}$ and for all $D \in \mathcal{D}_h^n$,

$$C_{\mathbf{S}, D}^n \mathbf{u} \cdot \mathbf{u} \geq \mathbf{S}(\mathbf{x}, t) \mathbf{u} \cdot \mathbf{u} \geq c_{\mathbf{S}, D}^n \mathbf{u} \cdot \mathbf{u}, \quad C_{\mathbf{S}, D}^n > 0, \quad c_{\mathbf{S}, D}^n > 0 \quad \forall \mathbf{u} \in \mathbb{R}^d$$

for a.e. $\mathbf{x} \in D$ and a.e. $t \in (t_{n-1}, t_n]$;

(A2) $\mathbf{v} \in \mathbf{L}^\infty(Q_T)$ such that $\nabla \cdot \mathbf{v} \in L^\infty(Q_T)$ such that for all $n \in \{1, \dots, N\}$ and for all $D \in \mathcal{D}_h^n$,

$$|\mathbf{v}(\mathbf{x}, t)| \leq C_{\mathbf{v}, D}^n, \quad C_{\mathbf{v}, D}^n \geq 0 \quad \text{for a.e. } \mathbf{x} \in D \text{ and a.e. } t \in (t_{n-1}, t_n];$$

(A3) $r \in L^\infty(Q_T)$;

(A4) For all $n \in \{1, \dots, N\}$ and for all $D \in \mathcal{D}_h^n$,

$$\begin{aligned} \frac{1}{2} \nabla \cdot \mathbf{v}(\mathbf{x}, t) + r(\mathbf{x}, t) &\geq c_{\mathbf{v}, r, D}^n, \quad \nabla \cdot \mathbf{v}(\mathbf{x}, t) + r(\mathbf{x}, t) \leq C_{\mathbf{v}, r, D}^n, \\ r(\mathbf{x}, t) &\leq C_{r, D}^n, \quad c_{\mathbf{v}, r, D}^n \geq 0, \quad C_{\mathbf{v}, r, D}^n \geq 0, \quad C_{r, D}^n \geq 0 \\ &\text{for a.e. } \mathbf{x} \in D \text{ and a.e. } t \in (t_{n-1}, t_n]; \end{aligned}$$

(A5) $f \in L^2(Q_T)$;

(A6) $u_0 \in L^\infty(\Omega)$;

(A7) if $c_{\mathbf{v}, r, D}^n = 0$, then $C_{\mathbf{v}, r, D}^n = 0$.

2.2 Continuous problem

Let us first define some functional spaces. Let $X := L^2(0, T; H_0^1(\Omega))$, $X' = L^2(0, T; H^{-1}(\Omega))$, and $Z := \{v \in X; v_t \in X'\}$. Let $v \in Z$. We define the functional $\mathcal{B}(v) \in X'$ by

$$\langle \mathcal{B}(v), \varphi \rangle := \langle v_t, \varphi \rangle + (\mathbf{S} \nabla v, \nabla \varphi) + (\nabla \cdot (v \mathbf{v}), \varphi) + (rv, \varphi) \quad (2.1)$$

for all $\varphi \in H_0^1(\Omega)$ and a.e. $t \in (0, T)$. Here $\langle \cdot, \cdot \rangle$ stands for the duality pairing between $H^{-1}(\Omega)$ and $H_0^1(\Omega)$ and (\cdot, \cdot) for the $L^2(\Omega)$ scalar product. We will also use $(\cdot, \cdot)_R$ for the $L^2(R)$ scalar product on a subdomain $R \subset \Omega$, $\langle \cdot, \cdot \rangle_R$ for the $L^2(R)$ scalar product on $R \subset \mathbb{R}^{d-1}$, and $|R|$ for the d' -dimensional Lebesgue measure of $R \subset \mathbb{R}^{d'}$, $d' \leq d$; at the same time, for a set R , $|R|$ stands for its cardinality.

We say that a function u is a weak solution of problem (1.1a)–(1.1c) if $u \in Z$, $u(\cdot, 0) = u_0$ in $H^{-1}(\Omega)$, and u satisfies the equality

$$\langle \mathcal{B}(u), \varphi \rangle = (f, \varphi) \quad (2.2)$$

for a.e. $t \in (0, T)$ and for all $\varphi \in H_0^1(\Omega)$. For a function $v \in X$, we introduce the space–time energy norm

$$\begin{aligned} \|v\|_X^2 &:= \int_0^T \|v(\cdot, t)\|^2 dt, \\ \|v\|^2 &:= \|\mathbf{S}^{\frac{1}{2}} \nabla v\|^2 + \|(\frac{1}{2} \nabla \cdot \mathbf{v} + r)^{\frac{1}{2}} v\|^2, \end{aligned} \quad (2.3)$$

where $\|\cdot\|$ denotes the $L^2(\Omega)$ norm. Assumption (A) then implies

$$\frac{1}{2} \|v(\cdot, T)\|^2 + \|v\|_X^2 \leq \int_0^T \langle \mathcal{B}(v), v \rangle dt + \frac{1}{2} \|v(\cdot, 0)\|^2 \quad \forall v \in Z. \quad (2.4)$$

Under Assumptions (A), there in particular exists a unique solution of (2.2).

Define, for $v \in Z$, the skew-symmetric part of the differential operator

$$b_A(v) := \nabla \cdot (v \mathbf{v}) - \frac{1}{2} (\nabla \cdot \mathbf{v}) v, \quad (2.5)$$

and, for all $\varphi \in H_0^1(\Omega)$ and a.e. $t \in (0, T)$, the symmetric and skew-symmetric parts of the functional \mathcal{B} , $\mathcal{B}_S(v), \mathcal{B}_A(v) \in X'$ by

$$\begin{aligned} \langle \mathcal{B}_S(v), \varphi \rangle &:= (\mathbf{S} \nabla v, \nabla \varphi) + ((\frac{1}{2} \nabla \cdot \mathbf{v} + r) v, \varphi), \\ \langle \mathcal{B}_A(v), \varphi \rangle &:= (b_A(v), \varphi). \end{aligned} \quad (2.6)$$

We will in the sequel also need a space Y , inspired by that of [25]: $Y := \{v \in X; \partial_t v + b_A(v) \in X'\}$ that we equip with its graph norm

$$\|v\|_Y^2 := \|v\|_X^2 + \|\partial_t v + b_A(v)\|_{X'}^2. \quad (2.7)$$

Recall that

$$\|\partial_t v + b_A(v)\|_{X'} = \sup_{\varphi \in X; \|\varphi\|_X=1} \int_0^T \langle \partial_t v + b_A(v), \varphi \rangle(t) dt.$$

We will also localize the $\|\cdot\|_X$ and $\|\cdot\|_Y$ norms on the time intervals $(t_{n-1}, t_n]$, $n \in \{1, \dots, N\}$, as follows:

$$\begin{aligned} \|v\|_{X(t_{n-1}, t_n)}^2 &:= \int_{t_{n-1}}^{t_n} \|v(\cdot, t)\|^2 dt, \\ \|v\|_{Y(t_{n-1}, t_n)}^2 &:= \|v\|_{X(t_{n-1}, t_n)}^2 + \|\partial_t v + b_A(v)\|_{X'(t_{n-1}, t_n)}^2. \end{aligned}$$

3 The combined finite volume–finite element method

We define in this section admissible grids and the combined finite volume–finite element scheme. This section can be skipped if the reader is only interested in a posteriori error estimates for conforming locally conservative methods and not in the details of the present scheme.

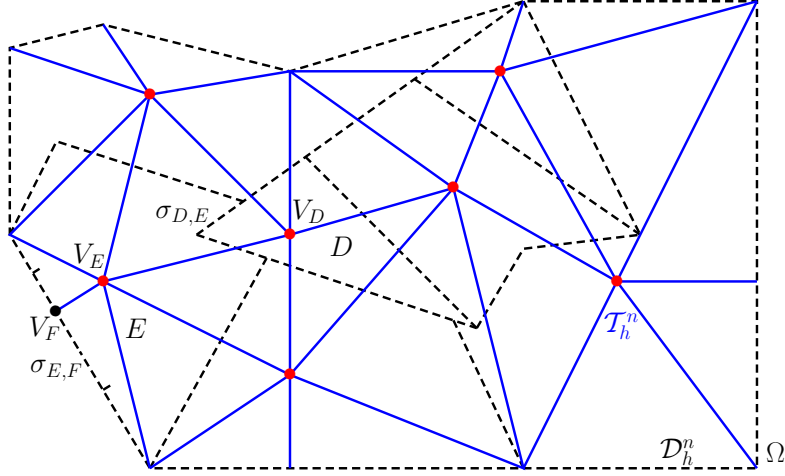


Figure 1: Primal nonmatching grid \mathcal{D}_h^n (dashed) and dual triangular grid \mathcal{T}_h^n (solid) with the elements $D, E \in \mathcal{D}_h^n$, points $V_D, V_E \in \mathcal{V}_h^{n,\text{int}}$ and $V_F \in \mathcal{V}_h^{n,\text{ext}}$, and sides $\sigma_{D,E} = \partial D \cap \partial E \in \mathcal{F}_h^{n,\text{int}}$ and $\sigma_{E,F} \in \mathcal{F}_h^{n,\text{ext}}$

3.1 Grids

We call the grid \mathcal{D}_h^n introduced in Section 2.1 a *primal grid* of Ω . In particular we admit non-matching grids, i.e., the case where there exist two different polygons $D, E \in \mathcal{D}_h^n$ such that their intersection is not an empty set but it is not a common vertex, edge, or face of D and E . We also allow for nonconvex elements and elements which are not star-shaped. An example of an admissible primal grid is given in Figure 1 by the dashed line. We suppose that there exists a family of points $\mathcal{V}_h^{n,\text{int}}$ such that there is one point V_D in the interior of D associated with each $D \in \mathcal{D}_h^n$. For $D \in \mathcal{D}_h^n$, we denote by \mathcal{F}_D the set of sides, subsets σ of ∂D such that there exists $E \in \mathcal{D}_h^n$ such that $\sigma = \sigma_{D,E} := \partial D \cap \partial E$ has a positive $(d-1)$ -dimensional Lebesgue measure. If there is a part of ∂D with a positive $(d-1)$ -dimensional Lebesgue measure lying on the boundary, then \mathcal{F}_D contains in addition a union of $\sigma = \sigma_{D,E} \subset \partial D \cap \partial \Omega$ covering $\partial D \cap \partial \Omega$ and such that each $\sigma_{D,E}$ has a positive $(d-1)$ -dimensional Lebesgue measure and contains exactly one point $V_E \in \mathcal{V}_h^{n,\text{ext}}$ defined below. We remark that $\partial D = \sum_{\sigma_{D,E} \in \mathcal{F}_D} \sigma_{D,E}$, that $\sigma_{D,E}$ is not necessarily a geometrical side of D , and that $\sigma_{D,E}$ not necessarily lies in a hyperplane of \mathbb{R}^d , see Figure 1. We denote by $\mathcal{F}_h^{n,\text{int}}$ the union of all $\sigma_{D,E} = \partial D \cap \partial E$ for some $D, E \in \mathcal{D}_h^n$, and by $\mathcal{F}_h^{n,\text{ext}}$ the union of all $\sigma \subset \partial \Omega$; all the sides of \mathcal{D}_h^n are then denoted by \mathcal{F}_h^n , $\mathcal{F}_h^n = \mathcal{F}_h^{n,\text{int}} \cup \mathcal{F}_h^{n,\text{ext}}$.

A *dual grid* of Ω is a partition \mathcal{T}_h^n of Ω into closed simplices which satisfies the following properties: (i) The set of points $\mathcal{V}_h^{n,\text{int}}$ is contained in the set of vertices of \mathcal{T}_h^n , denoted by \mathcal{V}_h^n ; (ii) The vertices from $\mathcal{V}_h^{n,\text{ext}} := \mathcal{V}_h^n \setminus \mathcal{V}_h^{n,\text{int}}$ lie on the boundary of Ω ; (iii) \mathcal{T}_h^n is conforming, i.e. the intersection of two different simplices is either an empty set or their common vertex, edge, or face; (iv) $\bar{\Omega} = \bigcup_{K \in \mathcal{T}_h^n} K$. This definition is not unique: we have a choice in connecting the different points $V_D \in \mathcal{V}_h^{n,\text{int}}$ and also a choice in the definition of the vertices on the boundary. The general intention is to find a triangulation \mathcal{T}_h^n such that the transmissibilities $\mathbb{S}_{D,E}^n$ defined below by (3.4) were non-negative, since this implies the discrete maximum principle, see Remark 3.2 below. We do not impose any requirement on the relation between the meshes \mathcal{D}_h^n and \mathcal{T}_h^n except of the assumption that the intersection of the sides of \mathcal{D}_h^n and \mathcal{T}_h^n has a zero $(d-2)$ -dimensional Lebesgue measure (the sides of \mathcal{D}_h^n and \mathcal{T}_h^n can intersect but not coincide). Example of a dual grid \mathcal{T}_h^n to the primal nonmatching grid \mathcal{D}_h^n is given in Figure 1 by the solid line. For a simplex

$K \in \mathcal{T}_h^n$, we denote by h_K its diameter. For a vertex $V_D \in \mathcal{V}_h^{n,\text{int}}$, we denote by $\mathcal{M}(V_D)$ the set of all vertices $V_E \in \mathcal{V}_h^n$ such that there exists an edge of the dual grid \mathcal{T}_h^n connecting V_D and V_E . Recall that each interior vertex from the set $\mathcal{V}_h^{n,\text{int}}$ is associated with one volume $D \in \mathcal{D}_h^n$ and that we use the notation V_D for this vertex. For the ease of notation, we denote each boundary vertex from the set $\mathcal{V}_h^{n,\text{ext}}$ by V_E , even if there is no corresponding volume $E \in \mathcal{D}_h^n$.

3.2 The combined scheme

The combined finite volume–finite element scheme is obtained, on each time level t_n , by the discretization of the diffusion term of (1.1a) by means of the piecewise affine conforming finite element method on the simplicial mesh \mathcal{T}_h^n , the discretization of the other terms of (1.1a) by means of the cell-centered finite volume method on the general polygonal/polyhedral partition \mathcal{D}_h^n , and using an implicit finite difference time stepping.

The scheme reads: find the values u_D^n , $n \in \{1, \dots, N\}$, $D \in \mathcal{D}_h^n$, such that

$$\frac{u_D^n - \bar{u}_D^{n-1}}{\tau_n} |D| - \sum_{V_E \in \mathcal{M}(V_D)} \mathbb{S}_{D,E}^n (u_E^n - u_D^n) + \sum_{\sigma_{D,E} \in \mathcal{F}_D} \langle \mathbf{v}^n \cdot \mathbf{n}, 1 \rangle_{\sigma_{D,E}} \bar{u}_{D,E}^n + r_D^n u_D^n |D| = f_D^n |D| \quad (3.1)$$

$$\forall n \in \{1, \dots, N\}, \forall D \in \mathcal{D}_h^n.$$

We now detail the notation used in (3.1).

We have set $u_E^n = 0$ for all $n \in \{1, \dots, N\}$ and all boundary vertices $V_E \in \mathcal{V}_h^{n,\text{ext}}$; this corresponds to the discretization of the homogeneous Dirichlet boundary condition (1.1c). The value \bar{u}_D^0 for D from the initial mesh \mathcal{D}_h^1 is given by $u_D^0 := (u_0, 1)_D / |D|$ and it corresponds to the discretization of the initial condition (1.1b). Let $n \geq 2$. When the meshes \mathcal{D}_h^{n-1} and \mathcal{D}_h^n (and \mathcal{T}_h^{n-1} and \mathcal{T}_h^n) coincide, we set $\bar{u}_D^{n-1} = u_D^{n-1}$, i.e., \bar{u}_D^{n-1} is the approximate solution u_D^{n-1} from the previous time step. In such a case the notation \bar{u}_D^{n-1} would not be necessary. This notation is introduced for the case where the meshes \mathcal{D}_h^{n-1} and \mathcal{D}_h^n (and \mathcal{T}_h^{n-1} and \mathcal{T}_h^n) are different. We then define \bar{u}_D^{n-1} by the value that the function u_h^{n-1} , defined by (3.8) below, takes at the point V_D corresponding to the volume $D \in \mathcal{D}_h^n$. In (3.1) and later on, \mathbf{n} stands for the unit normal vector of ∂D , outward to D .

Let the averages in time of the functions f , r , \mathbf{v} , and \mathbf{S} be respectively given by

$$\begin{aligned} f^n(\mathbf{x}) &:= \frac{1}{\tau_n} \int_{t_{n-1}}^{t_n} f(\mathbf{x}, t) dt && \text{for a.e. } \mathbf{x} \in \Omega, n \in \{1, \dots, N\}, \\ r^n(\mathbf{x}) &:= \frac{1}{\tau_n} \int_{t_{n-1}}^{t_n} r(\mathbf{x}, t) dt && \text{for a.e. } \mathbf{x} \in \Omega, n \in \{1, \dots, N\}, \\ \mathbf{v}^n(\mathbf{x}) &:= \frac{1}{\tau_n} \int_{t_{n-1}}^{t_n} \mathbf{v}(\mathbf{x}, t) dt && \text{for a.e. } \mathbf{x} \in \Omega, n \in \{1, \dots, N\}, \\ \mathbf{S}^n(\mathbf{x}) &:= \frac{1}{\tau_n} \int_{t_{n-1}}^{t_n} \mathbf{S}(\mathbf{x}, t) dt && \text{for a.e. } \mathbf{x} \in \Omega, n \in \{1, \dots, N\}. \end{aligned}$$

In (3.1), we have also set

$$f_D^n := \frac{(f^n, 1)}{|D|} \quad n \in \{1, \dots, N\}, D \in \mathcal{D}_h^n, \quad (3.2)$$

$$r_D^n := \frac{(r^n, 1)}{|D|} \quad n \in \{1, \dots, N\}, D \in \mathcal{D}_h^n. \quad (3.3)$$

The notation \mathbb{S} in (3.1) stands for the finite element diffusion matrix; the elements $\mathbb{S}_{D,E}^n$, $V_D \in \mathcal{V}_h^{n,\text{int}}$, $V_E \in \mathcal{V}_h^n$ are given by

$$\mathbb{S}_{D,E}^n := - \sum_{K \in \mathcal{T}_h^n} (\mathbf{S}_h^n \nabla \psi_{V_E}, \nabla \psi_{V_D})_K \quad n \in \{1, \dots, N\}. \quad (3.4)$$

Here ψ_{V_D} is the finite element basis function associated with the vertex $V_D \in \mathcal{V}_h^n$: it is the function piecewise affine on the simplicial mesh \mathcal{T}_h^n , equal to 1 at the vertex V_D , and equal to zero at all other vertices $V_E \in \mathcal{V}_h^n$. In (3.4), the notation \mathbf{S}_h^n for the space–time discrete diffusion–dispersion tensor appears. There are two basic choices for \mathbf{S}_h^n : Firstly, we may set

$$\mathbf{S}_h^n|_K := \frac{1}{|K|} (\mathbf{S}^n, 1)_K \quad n \in \{1, \dots, N\}, K \in \mathcal{T}_h^n. \quad (3.5)$$

Note that since $\nabla \psi_{V_D}, \nabla \psi_{V_E}$ in (3.4) are constant on all $K \in \mathcal{T}_h^n$, the definition (3.5) is equivalent to directly using $\mathbf{S}_h^n = \mathbf{S}^n$ in (3.4). An alternative choice is to define \mathbf{S}_h^n by

$$\mathbf{S}_h^n|_K := \left(\frac{1}{|K|} ([\mathbf{S}^n]^{-1}, 1)_K \right)^{-1} \quad n \in \{1, \dots, N\}, K \in \mathcal{T}_h^n. \quad (3.6)$$

We refer to Remark 3.3 below for the discussion of these two choices.

We finally turn to the description of the discretization of the convection term in (3.1). We define the value $\overline{u_{D,E}^n}$, used for the evaluation of the convective flux across a side $\sigma_{D,E} \in \mathcal{F}_h^n$, $n \in \{1, \dots, N\}$, $D \in \mathcal{D}_h^n$, by

$$\overline{u_{D,E}^n} := \begin{cases} u_D^n + \alpha_{D,E}^n (u_E^n - u_D^n) & \text{if } \langle \mathbf{v}^n \cdot \mathbf{n}, 1 \rangle_{\sigma_{D,E}} \geq 0 \\ u_E^n + \alpha_{D,E}^n (u_D^n - u_E^n) & \text{if } \langle \mathbf{v}^n \cdot \mathbf{n}, 1 \rangle_{\sigma_{D,E}} < 0 \end{cases}. \quad (3.7)$$

Here $\alpha_{D,E}^n$ is the coefficient of the amount of upstream weighting which is defined by

$$\alpha_{D,E}^n := \begin{cases} \frac{\max\{\min\{\mathbb{S}_{D,E}^n, \frac{1}{2} |\langle \mathbf{v}^n \cdot \mathbf{n}, 1 \rangle_{\sigma_{D,E}}|\}, 0\}}{|\langle \mathbf{v}^n \cdot \mathbf{n}, 1 \rangle_{\sigma_{D,E}}|} & \text{if } \langle \mathbf{v}^n \cdot \mathbf{n}, 1 \rangle_{\sigma_{D,E}} \neq 0 \text{ and } \sigma_{D,E} \in \mathcal{F}_h^{n,\text{int}} \\ & \text{or if } \sigma_{D,E} \in \mathcal{F}_h^{n,\text{ext}} \text{ and } \langle \mathbf{v}^n \cdot \mathbf{n}, 1 \rangle_{\sigma_{D,E}} > 0 \\ 0 & \text{if } \langle \mathbf{v}^n \cdot \mathbf{n}, 1 \rangle_{\sigma_{D,E}} = 0 \text{ or if } \sigma_{D,E} \in \mathcal{F}_h^{n,\text{ext}} \\ & \text{and } \langle \mathbf{v}^n \cdot \mathbf{n}, 1 \rangle_{\sigma_{D,E}} < 0 \end{cases}.$$

By such a definition, the value $\overline{u_{D,E}^n}$ ranges between the upstream value and the centered one, in function of the size and direction of the convective field \mathbf{v} .

The scheme (3.1) yields the discrete values u_D^n , $n \in \{0, \dots, N\}$, $D \in \mathcal{D}_h^n$. These values define, for each $n \in \{0, \dots, N\}$, the usual finite element approximation u_h^n , piecewise affine on the simplicial mesh \mathcal{T}_h^n , given by the formula

$$u_h^n := \sum_{D \in \mathcal{D}_h^n} u_D^n \psi_{V_D}. \quad (3.8)$$

By the approximate solution of problem (1.1a)–(1.1c) by means of the combined finite volume–finite element scheme (3.1), we understand a function $u_{h,\tau}$ such that

$$\begin{aligned} u_{h,\tau}(\cdot, t_n) &:= u_h^n \quad n \in \{0, \dots, N\}, \\ u_{h,\tau}(\mathbf{x}, \cdot) &\text{ is affine in time on } [t_{n-1}, t_n], \quad n \in \{1, \dots, N\}, \text{ for all } \mathbf{x} \in \Omega. \end{aligned} \quad (3.9)$$

3.3 Remarks

We end this section by several remarks.

Remark 3.1 (Convergence). *The convergence of $u_{h,\tau}$ towards the weak solution of problem (1.1a)–(1.1c) given by (2.2) has been proved in [13]. Herein, a more general nonlinear degenerate case has been considered, under the assumption that the meshes $\mathcal{D}_h^n, \mathcal{T}_h^n$ do not change in time.*

Remark 3.2 (Discrete maximum principle). *If the finite element diffusion matrix entries $\mathbb{S}_{D,E}^n$ satisfy $\mathbb{S}_{D,E}^n \geq 0$ for all $n \in \{1, \dots, N\}$, $D \in \mathcal{D}_h^n$, and $V_E \in \mathcal{M}(V_D)$, and under suitable conditions on the data, the discrete maximum principle for the combined scheme holds, see [13, Theorem 4.11].*

Remark 3.3 (Arithmetic versus harmonic averaging). *We remark that the choice (3.5) for space–time discrete diffusion–dispersion tensor \mathbf{S}_h^n corresponds to the arithmetic average of the diffusion–dispersion tensor \mathbf{S}^n in space, whereas the choice (3.6) corresponds to the harmonic average in space.*

Remark 3.4 (Relation to the vertex-centered finite volume method). *Let the meshes \mathcal{T}_h^n be given first and let the meshes \mathcal{D}_h^n be constructed consequently from \mathcal{T}_h^n using the face, edge, and element barycentres of \mathcal{T}_h^n , cf., e.g., [19, 31]. Then the combined finite volume–finite element scheme (3.1) is equivalent to the classical vertex-centered finite volume method (cf., e.g., [19] and the references therein), where mass lumping has been used in the time evolution and reaction terms. Hence, all the results of the present paper apply to the vertex-centered finite volume method as a special case with specific construction of \mathcal{D}_h^n from \mathcal{T}_h^n .*

4 A posteriori error estimate and its efficiency

We summarize in this section our a posteriori estimate on the error between the weak solution u and the approximate solution $u_{h,\tau}$ and the efficiency of this estimate. The developments of this section are done generally, without specification of the underlying numerical scheme. We merely suppose that Assumption (B) below holds for the upper bounds of Section 4.4 and that Assumption (C) below holds for the lower bound of Section 4.6.

4.1 Some useful inequalities

We summarize here some inequalities that will be used later.

Let $D \subset \mathbb{R}^d$ be a polygon. The Poincaré inequality states that

$$\|\varphi - \varphi_D\|_D^2 \leq C_{P,D} h_D^2 \|\nabla \varphi\|_D^2 \quad \forall \varphi \in H^1(D), \quad (4.1)$$

where φ_D is the mean of the function φ over the polygon D given by $\varphi_D := (\varphi, 1)_D / |D|$ and where h_D is the diameter of D . The constant $C_{P,D}$ can be evaluated as $1/\pi^2$ if D is convex, cf. [20, 3], and only depends on the geometry of D if D is nonconvex, cf. [12, Lemma 10.4].

Let $D \subset \mathbb{R}^d$ be a polygon near the boundary of Ω , such that $|\partial\Omega \cap \partial D| \neq 0$. Then the Friedrichs inequality states that

$$\|\varphi\|_D^2 \leq C_{F,D,\partial\Omega} h_D^2 \|\nabla \varphi\|_D^2 \quad \forall \varphi \in H^1(D) \text{ such that } \varphi = 0 \text{ on } \partial\Omega \cap \partial D. \quad (4.2)$$

As long as D and $\partial\Omega$ are such that there exists a vector $\mathbf{b} \in \mathbb{R}^d$ such that for almost all $\mathbf{x} \in D$, the first intersection of $\mathcal{B}_{\mathbf{x}}$ and ∂D lies in $\partial\Omega$, where $\mathcal{B}_{\mathbf{x}}$ is the straight semi-line defined by the origin \mathbf{x} and the vector \mathbf{b} , the constant $C_{F,D,\partial\Omega}$ can be evaluated as 1, cf. [28, Remark 5.8]. To evaluate

$C_{F,D,\partial\Omega}$ in the general case is more complicated but it still can be done, cf. [28, Remark 5.9] or [5, Section 3]. As a special case, when $D = \Omega$, the Friedrichs inequality reads

$$\|\varphi\|^2 \leq C_F h_\Omega^2 \|\nabla\varphi\|^2 \quad \forall \varphi \in H_0^1(\Omega), \quad (4.3)$$

and $C_F = 1$.

Finally, for a simplex $K \subset \mathbb{R}^d$, the trace inequality states that

$$\|\varphi\|_\sigma^2 \leq C_{t,K,\sigma} (h_K^{-1} \|\varphi\|_K^2 + \|\varphi\|_K \|\nabla\varphi\|_K) \quad \forall \varphi \in H^1(K). \quad (4.4)$$

It follows from [22, Lemma 3.12] that the constant $C_{t,K,\sigma}$ can be evaluated as $|\sigma| h_K / |K|$.

4.2 Some additional notation

Let, for $n \in \{1, \dots, N\}$, \mathcal{D}_h^n and \mathcal{T}_h^n be the primal and dual meshes as introduced in Section 3.1. For $n \in \{2, \dots, N\}$, let $\mathcal{S}_h^{n-1,n}$ be an additional tertial simplicial mesh, a conforming refinement of all \mathcal{D}_h^{n-1} , \mathcal{D}_h^n , \mathcal{T}_h^{n-1} , and \mathcal{T}_h^n . Let, for $n = 1$, $\mathcal{S}_h^{0,1}$ be a simplicial conforming refinement of both \mathcal{D}_h^1 and \mathcal{T}_h^1 . An example of the three types of meshes \mathcal{D}_h^n , \mathcal{T}_h^n , and $\mathcal{S}_h^{n-1,n}$ is given in Figure 2 below. We denote by \mathcal{S}_D the partition of $D \in \mathcal{D}_h^n$ by the elements of $\mathcal{S}_h^{n-1,n}$. Let $K \in \mathcal{S}_h^{n-1,n}$ be a generic element of $\mathcal{S}_h^{n-1,n}$. We denote by \mathcal{G}_K its sides and by $\mathcal{G}_K^{\text{int}}$ its sides not contained in $\partial\Omega$. By \mathcal{G}_D , we denote all the sides of the partition \mathcal{S}_D for a given volume D , except those sides included in the boundary $\partial\Omega$. We will also use the notation $\mathcal{S}_h^{n-1,n,\text{int}}$ and $\mathcal{S}_h^{n-1,n,\text{ext}}$ for the simplices of $\mathcal{S}_h^{n-1,n}$ in the interior of Ω and having a side on the boundary of Ω , respectively.

Let X_h denote the space of scalar functions continuous in space and piecewise affine on the meshes $\mathcal{S}_h^{n-1,n}$ and piecewise affine and continuous in time. A function $v_h \in X_h$ is, as in (3.9), uniquely prescribed by the functions v_h^n defined on the meshes $\mathcal{S}_h^{n-1,n}$ and by the function v_h^0 defined on $\mathcal{S}_h^{0,1}$. Recall that v_h^n stands for the value of the function v_h at the times t_n , $n \in \{0, \dots, N\}$. Typically, the values u_D^n , $D \in \mathcal{D}_h^n$, $n \in \{0, \dots, N\}$, define through (3.8)–(3.9) the function $u_{h,\tau} \in X_h$.

We finally denote by \mathbf{V}_h the space of vector functions which are such that they belong to the Raviart–Thomas–Nédélec spaces of lowest order (cf. [4]) on the meshes $\mathcal{S}_h^{n-1,n}$ in space and which are piecewise constant in time. A function $\mathbf{u}_h \in \mathbf{V}_h$ is uniquely prescribed by the functions \mathbf{u}_h^n defined on the meshes $\mathcal{S}_h^{n-1,n}$, the values of \mathbf{u}_h on the time intervals $(t_{n-1}, t_n]$, $n \in \{1, \dots, N\}$. Recall that the normal components of the functions \mathbf{u}_h from the space \mathbf{V}_h are continuous ([4]); the values $\mathbf{u}_h^n \cdot \mathbf{n} | \sigma | = \langle \mathbf{u}_h^n \cdot \mathbf{n}, 1 \rangle_\sigma$ on the sides σ of the meshes $\mathcal{S}_h^{n-1,n}$, $n \in \{1, \dots, N\}$, represent the degrees of freedom in the space \mathbf{V}_h .

4.3 Diffusive and convective flux reconstructions

Following [29, 31, 11], our a posteriori error estimates rely on the concept of the *diffusive flux reconstruction* $\boldsymbol{\theta}_h \in \mathbf{V}_h$. Following [10], we also introduce a *convective flux reconstruction* $\mathbf{w}_h \in \mathbf{V}_h$. In order to proceed generally for the upper bounds of Section 4.4 below, without the specification of a particular numerical scheme, we now make the following assumption:

Assumption (B) (Local conservativity of the numerical scheme)

We suppose that there exist values u_D^n , $n \in \{0, \dots, N\}$, $D \in \mathcal{D}_h^n$, values \bar{u}_D^{n-1} , $n \in \{1, \dots, N\}$, $D \in \mathcal{D}_h^n$, and functions $\boldsymbol{\theta}_h, \mathbf{w}_h \in \mathbf{V}_h$ such that

$$\frac{u_D^n - \bar{u}_D^{n-1}}{\tau_n} |D| + \langle \boldsymbol{\theta}_h^n \cdot \mathbf{n}, 1 \rangle_{\partial D} + \langle \mathbf{w}_h^n \cdot \mathbf{n}, 1 \rangle_{\partial D} + r_D^n u_D^n |D| + q_D^n |D| = f_D^n |D| \quad (4.5)$$

$$\forall n \in \{1, \dots, N\}, \forall D \in \mathcal{D}_h^n.$$

In Assumption (B), r_D^n and f_D^n are given by (3.2)–(3.3). Relation (4.5) is a local conservation property: the term $(u_D^n - \bar{u}_D^{n-1})|D|/\tau_n$ represents the time accumulation in the volume D , $\langle \boldsymbol{\theta}_h^n \cdot \mathbf{n}, 1 \rangle_{\partial D}$ the diffusive flux over the boundary ∂D , $\langle \mathbf{w}_h^n \cdot \mathbf{n}, 1 \rangle_{\partial D}$ the convective flux over ∂D , and $r_D^n u_D^n |D|$ and $f_D^n |D|$, respectively, the reaction and sources accumulation in the volume D . Finally, the term $q_D^n |D|$ represents a quadrature error term. This term may not be present at all (this is a typical situation for vertex-centered finite volume schemes). It appears when the local conservation is not satisfied exactly for the numerical scheme in question.

A vast class of locally conservative methods enters the framework of Assumption (B). In particular, the combined finite volume–finite element scheme (3.1) can be written in the form (4.5) with

$$\langle \boldsymbol{\theta}_h^n \cdot \mathbf{n}, 1 \rangle_\sigma := -\langle \mathbf{S}_h^n \nabla u_h^n \cdot \mathbf{n}, 1 \rangle_\sigma \quad \sigma \subset \partial D, D \in \mathcal{D}_h^n, \quad (4.6)$$

where σ stands for a side of a simplex K from the partition \mathcal{S}_D of the volume D which is such that $\sigma \subset \partial D$, and

$$\langle \mathbf{w}_h^n \cdot \mathbf{n}, 1 \rangle_{\sigma_{D,E}} := \langle \mathbf{v}^n \cdot \mathbf{n}, 1 \rangle_{\sigma_{D,E}} \overline{u_{D,E}^n} \quad \sigma_{D,E} \in \mathcal{F}_D, D \in \mathcal{D}_h^n, \quad (4.7)$$

where, recall from Section 3.1, $\sigma_{D,E}$ stands for a side of the volume D . The diffusive fluxes $\langle \boldsymbol{\theta}_h \cdot \mathbf{n}, 1 \rangle_\sigma$ given by (4.6) do not necessarily coincide completely with those stemming from the combined scheme (3.1) on general meshes \mathcal{D}_h^n . Then, the quadrature factor $q_D^n |D|$ is nonzero and fixes the balance. In numerical experiments in Section 7 below, the values $q_D^n |D|$ defined in this way were completely negligible. We finally remark that equations (4.6) and (4.7) do not prescribe the diffusive and convective fluxes $\boldsymbol{\theta}_h$ and \mathbf{w}_h uniquely; they are sufficient, altogether with Assumption (C) below, for the present theoretical analysis. For a practical implementation, there exist several possibilities for fixing the remaining degrees of freedom of $\boldsymbol{\theta}_h$ and \mathbf{w}_h . We refer to [31, Section 4.3] for the details and examples of these possibilities.

4.4 A posteriori error estimate

In this section, we derive our a posteriori error estimate. We suppose that the approximate solution $u_{h,\tau}$ belongs to the space X_h and that there are diffusive and convective flux reconstructions $\boldsymbol{\theta}_h$ and \mathbf{w}_h belonging to the space \mathbf{V}_h , arbitrary but such that Assumption (B) holds. A particular example entering such a framework is the combined finite volume–finite element scheme (3.1) with the construction of $\boldsymbol{\theta}_h$ and \mathbf{w}_h by (4.6)–(4.7).

Let $n \in \{1, \dots, N\}$ and let D be a volume of the mesh \mathcal{D}_h^n . We first define a multiplicative cutoff factor

$$m_D^n := \min \left\{ C_{P,D}^{\frac{1}{2}} h_D (c_{\mathbf{S},D}^n)^{-\frac{1}{2}}, (c_{\mathbf{v},r,D}^n)^{-\frac{1}{2}} \right\},$$

where the constants $c_{\mathbf{S},D}^n$ and $c_{\mathbf{v},r,D}^n$ are specified in Assumption (A), $C_{P,D}$ is the constant from the Poincaré inequality (4.1), and h_D is the diameter of the volume D . We then define the *residual estimator* $\eta_{R,D}^n$ by

$$\eta_{R,D}^n := m_D^n \left\| f_D^n - \frac{u_D^n - \bar{u}_D^{n-1}}{\tau_n} - \nabla \cdot \boldsymbol{\theta}_h^n - \nabla \cdot \mathbf{w}_h^n - r_D^n u_D^n - q_D^n \right\|_D. \quad (4.8)$$

The *diffusive and convective flux estimator* $\eta_{DCF,D}^n$ is given by

$$\eta_{DCF,D}^n(t) := \left\| \mathbf{S}^{\frac{1}{2}} \nabla u_{h,\tau} + \mathbf{S}^{-\frac{1}{2}} \boldsymbol{\theta}_h^n - \mathbf{S}^{-\frac{1}{2}} u_{h,\tau} \mathbf{v} + \mathbf{S}^{-\frac{1}{2}} \mathbf{w}_h^n \right\|_D(t). \quad (4.9)$$

Let K be a simplex from the tertial mesh $\mathcal{S}_h^{n-1,n}$. We then define the multiplicative cutoff factors

$$m_K^n := \min\left\{C_{\text{P},\text{F},K}^{\frac{1}{2}} h_K (c_{\mathbf{S},K}^n)^{-\frac{1}{2}}, (c_{\mathbf{v},r,K}^n)^{-\frac{1}{2}}\right\}, \quad (4.10a)$$

$$\tilde{m}_K^n := \min\left\{(C_{\text{P},\text{F},K} + C_{\text{P},\text{F},K}^{\frac{1}{2}}) h_K (c_{\mathbf{S},K}^n)^{-1}, h_K^{-1} (c_{\mathbf{v},r,K}^n)^{-1} + \frac{1}{2} (c_{\mathbf{v},r,K}^n)^{-\frac{1}{2}} (c_{\mathbf{S},K}^n)^{-\frac{1}{2}}\right\}, \quad (4.10b)$$

where $C_{\text{P},\text{F},K} := C_{\text{P},K}$ for $K \in \mathcal{S}_h^{n-1,n,\text{int}}$ and $C_{\text{P},\text{F},K} := C_{\text{F},K,\partial\Omega}$ for $K \in \mathcal{S}_h^{n-1,n,\text{ext}}$ are the constants from the Poincaré/Friedrichs inequalities (4.1) or (4.2), the constants $c_{\mathbf{S},K}^n$ and $c_{\mathbf{v},r,K}^n$ are specified in Assumption (A), and h_K is the diameter of K . We will need below also the *diffusive flux estimator* $\eta_{\text{DF},D}^n$

$$\begin{aligned} \eta_{\text{DF},D}^n(t) := & \left\{ \sum_{K \in \mathcal{S}_D} \left(m_K^n \|\nabla \cdot (\mathbf{S}\nabla u_{h,\tau} + \boldsymbol{\theta}_h^n)\|_K \right. \right. \\ & \left. \left. + (\tilde{m}_K^n)^{\frac{1}{2}} \sum_{\sigma \in \mathcal{G}_K^{\text{int}}} (C_{t,K,\sigma})^{\frac{1}{2}} \|(\mathbf{S}\nabla u_{h,\tau} + \boldsymbol{\theta}_h^n) \cdot \mathbf{n}\|_{\sigma} \right)^2 \right\}^{\frac{1}{2}} (t). \end{aligned} \quad (4.11)$$

Next, define the multiplicative cutoff factor

$$\bar{m}^n := \min\left\{C_{\text{F}}^{\frac{1}{2}} h_{\Omega} (c_{\mathbf{S},\Omega}^n)^{-\frac{1}{2}}, (c_{\mathbf{v},r,\Omega}^n)^{-\frac{1}{2}}\right\},$$

where $C_{\text{F}} = 1$ is the constant from the Friedrichs inequality (4.3), $c_{\mathbf{S},\Omega}^n$ and $c_{\mathbf{v},r,\Omega}^n$ are specified in Assumption (A), and h_{Ω} is the diameter of Ω . Then the *data oscillation–quadrature estimator* $\eta_{\text{DOQ},D}^n$ is given by

$$\eta_{\text{DOQ},D}^n(t) := \bar{m}^n \left\| f - f_D^n - (u_{h,\tau})_t + \frac{u_D^n - \bar{u}_D^{n-1}}{\tau_n} - r u_{h,\tau} + r_D^n u_D^n + q_D^n \right\|_D (t). \quad (4.12)$$

We finally denote

$$\begin{aligned} (\eta^{(1),n})^2 &:= \int_{t_{n-1}}^{t_n} \left(\left\{ \sum_{D \in \mathcal{D}_h^n} (\eta_{\text{R},D}^n + \eta_{\text{DCF},D}^n(t))^2 \right\}^{\frac{1}{2}} + \left\{ \sum_{D \in \mathcal{D}_h^n} (\eta_{\text{DOQ},D}^n(t))^2 \right\}^{\frac{1}{2}} \right)^2 dt, \\ (\eta^{(2),n})^2 &:= \int_{t_{n-1}}^{t_n} \left(\left\{ \sum_{D \in \mathcal{D}_h^n} (\eta_{\text{R},D}^n)^2 \right\}^{\frac{1}{2}} + \left\{ \sum_{D \in \mathcal{D}_h^n} (\eta_{\text{DF},D}^n(t))^2 \right\}^{\frac{1}{2}} \right. \\ &\quad \left. + \sup_{\varphi \in H_0^1(\Omega); \|\varphi\|=1} (\nabla \cdot (u_{h,\tau} \mathbf{v} - \mathbf{w}_h^n), \varphi) + \left\{ \sum_{D \in \mathcal{D}_h^n} (\eta_{\text{DOQ},D}^n(t))^2 \right\}^{\frac{1}{2}} \right)^2 dt \end{aligned}$$

and

$$\eta^n := \min\{\eta^{(1),n}, \eta^{(2),n}\}, \quad (4.13a)$$

$$\eta := \left\{ \sum_{n=1}^N (\eta^n)^2 \right\}^{\frac{1}{2}}. \quad (4.13b)$$

Using these definitions, we will prove in Section 5.1 below the following a posteriori error estimate:

Theorem 4.1 (Energy norm a posteriori error estimate). *Let u be the weak solution of problem (1.1a)–(1.1c) given by (2.2) and let $u_{h,\tau} \in X_h$ and $\boldsymbol{\theta}_h, \mathbf{w}_h \in \mathbf{V}_h$ be arbitrary but such that Assumption (B) holds. Then*

$$\|(u - u_{h,\tau})(\cdot, T)\|^2 + \|u - u_{h,\tau}\|_X^2 \leq \eta^2 + \|u_0 - u_{h,\tau}(\cdot, 0)\|^2.$$

Theorem 4.2 (Augmented norm a posteriori error estimate). *Let the assumptions of Theorem 4.1 hold. Then*

$$3\|(u - u_{h,\tau})(\cdot, T)\|^2 + \|u - u_{h,\tau}\|_Y^2 \leq 5\eta^2 + 3\|u_0 - u_{h,\tau}(\cdot, 0)\|^2.$$

Remark 4.3 (Estimators $\eta^{(1),n}$). *We remark that the estimators $\eta^{(1),n}$ give a guaranteed upper bound. They are also fully and locally computable in the sense that they are based on an evaluation of certain quantities accessible locally in the mesh cells. Remark also that their principal parts (cf. the numerical experiments of Section 7 below) are given by the constant-free estimators (4.9).*

Remark 4.4 (Estimators $\eta^{(2),n}$). *The estimators $\eta^{(1),n}$ themselves would not be robust with respect to the convection or reaction dominance, cf. [7, 27]. This is the reason for also introducing the estimators $\eta^{(2),n}$. Using these estimators, robust lower bound will be proven in Theorem 4.7 below, following [25]. The disadvantage of the estimators $\eta^{(2),n}$ is, however, that they are not computable, as they feature the supremum over all function $\varphi \in H_0^1(\Omega)$ with $\|\varphi\| = 1$. Computable upper bounds on $\eta^{(2),n}$, still ensuring robustness, can be established following [25, Section 8]. The price to pay is a solution of an auxiliary stationary reaction–diffusion problem on each time step. Such an approach is not computationally pursued here in view of its complexity.*

Remark 4.5 (Data oscillation–quadrature estimators). *In a posteriori estimates for finite element, vertex-centered finite volume, or mixed finite element methods, cf. [25, 11], data oscillation estimators of the form $\overline{m}^n \|f - f_D^n\|$ appear. The other terms of the present estimators $\eta_{\text{DOQ},D}^n$ (4.12) are related to the non-variational general nature of (4.5) (or of (3.1)). They correspond to a numerical quadrature error; this is illustrated in Section 7 below on numerical experiments. If the vertex-centered finite volume method, cf., e.g. [19], was used instead of (4.5), then the estimators $\eta_{\text{DOQ},D}^n$ would reduce to the usual data oscillation estimators $\overline{m}^n \|f - f_D^n\|$.*

4.5 Distinguishing the space and time error contributions

The estimate $\eta^{(1),n}$ of (4.13a) is fully computable and allows to control the overall error. There is, however, no distinction between the space and time errors. Using the triangle inequality, we have, as in [11], for the example of $\eta_{\text{DCF},D}^n(t)$,

$$\begin{aligned} \eta_{\text{DCF},D}^n(t) &\leq \left\| \mathbf{S}^{\frac{1}{2}} \nabla u_h^n + \mathbf{S}^{-\frac{1}{2}} \boldsymbol{\theta}_h^n - \mathbf{S}^{-\frac{1}{2}} u_h^n \mathbf{v}^n + \mathbf{S}^{-\frac{1}{2}} \mathbf{w}_h^n \right\|_D(t) \\ &\quad + \left\| \mathbf{S}^{\frac{1}{2}} \nabla u_{h,\tau} - \mathbf{S}^{\frac{1}{2}} \nabla u_h^n - \mathbf{S}^{-\frac{1}{2}} u_{h,\tau} \mathbf{v} + \mathbf{S}^{-\frac{1}{2}} u_h^n \mathbf{v}^n \right\|_D(t). \end{aligned}$$

Note that whenever \mathbf{S} is constant in time on $(t_{n-1}, t_n]$, the first of the above terms gets independent of time; it clearly corresponds to the spatial part of the error. The second of the above terms then corresponds to the temporal part of the error, so that we have the usual space–time contributions division as in [21, 25]. Note as well that when both \mathbf{S} and \mathbf{v} are constant in time on $(t_{n-1}, t_n]$, we get, using the definition of $u_{h,\tau}$ by (3.9) as in [24, Equation (6.5)], the following easily computable

upper bound on $\left\{ \int_{t_{n-1}}^{t_n} (\eta_{\text{DCF},D}^n(t))^2 dt \right\}^{\frac{1}{2}}$:

$$\begin{aligned} \left\{ \int_{t_{n-1}}^{t_n} (\eta_{\text{DCF},D}^n(t))^2 dt \right\}^{\frac{1}{2}} &\leq \tau_n^{\frac{1}{2}} \left\| (\mathbf{S}^n)^{\frac{1}{2}} \nabla u_h^n + (\mathbf{S}^n)^{-\frac{1}{2}} \boldsymbol{\theta}_h^n - (\mathbf{S}^n)^{-\frac{1}{2}} u_h^n \mathbf{v}^n + (\mathbf{S}^n)^{-\frac{1}{2}} \mathbf{w}_h^n \right\|_D \\ &\quad + \left(\frac{\tau_n}{3} \right)^{\frac{1}{2}} \left\| (\mathbf{S}^n)^{\frac{1}{2}} \nabla (u_h^{n-1} - u_h^n) - (\mathbf{S}^n)^{-\frac{1}{2}} \mathbf{v}^n (u_h^{n-1} - u_h^n) \right\|_D. \end{aligned}$$

We now proceed similarly for the other estimators, for general \mathbf{S} and \mathbf{v} . We obtain

$$\eta^n \leq \eta_{\text{sp}}^n + \eta_{\text{tm}}^n$$

with

$$\begin{aligned} \eta_{\text{sp}}^n &:= \left\{ \tau_n \sum_{D \in \mathcal{D}_h^n} (\eta_{\text{R},D}^n)^2 \right\}^{\frac{1}{2}} + \left\{ \int_{t_{n-1}}^{t_n} \sum_{D \in \mathcal{D}_h^n} \left\| \mathbf{S}^{\frac{1}{2}} \nabla u_h^n + \mathbf{S}^{-\frac{1}{2}} \boldsymbol{\theta}_h^n - \mathbf{S}^{-\frac{1}{2}} u_h^n \mathbf{v}^n + \mathbf{S}^{-\frac{1}{2}} \mathbf{w}_h^n \right\|_D^2(t) dt \right\}^{\frac{1}{2}} \\ &\quad + \left\{ \int_{t_{n-1}}^{t_n} \sum_{D \in \mathcal{D}_h^n} (\overline{m}^n)^2 \left\| f - f_h - (u_{h,\tau})_t + \frac{u_D^n - \bar{u}_D^{n-1}}{\tau_n} - r^n u_h^n + r_D^n u_D^n + q_D^n \right\|_D^2(t) dt \right\}^{\frac{1}{2}} \end{aligned} \quad (4.14)$$

and

$$\begin{aligned} \eta_{\text{tm}}^n &:= \left\{ \int_{t_{n-1}}^{t_n} \sum_{D \in \mathcal{D}_h^n} \left\| \mathbf{S}^{\frac{1}{2}} \nabla u_{h,\tau} - \mathbf{S}^{\frac{1}{2}} \nabla u_h^n - \mathbf{S}^{-\frac{1}{2}} u_{h,\tau} \mathbf{v} + \mathbf{S}^{-\frac{1}{2}} u_h^n \mathbf{v}^n \right\|_D^2(t) dt \right\}^{\frac{1}{2}} \\ &\quad + \left\{ \int_{t_{n-1}}^{t_n} \sum_{D \in \mathcal{D}_h^n} (\overline{m}^n)^2 \left\| f_h - f_D^n - r u_{h,\tau} + r^n u_h^n \right\|_D^2(t) dt \right\}^{\frac{1}{2}}. \end{aligned} \quad (4.15)$$

Consequently, we have the following corollary:

Corollary 4.6 (Energy norm a posteriori error estimate distinguishing the space and time errors). *Let the assumptions of Theorem 4.1 hold. Then*

$$\|(u - u_{h,\tau})(\cdot, T)\|^2 + \|u - u_{h,\tau}\|_X^2 \leq \sum_{n=1}^N (\eta_{\text{sp}}^n + \eta_{\text{tm}}^n)^2 + \|(u - u_{h,\tau})(\cdot, 0)\|^2.$$

4.6 Efficiency of the estimate

For the sake of simplicity, we make in this section an additional assumption that $\nabla \cdot \mathbf{v} = 0$. In this case, the augmented norm (2.7) is closely related to that of [25], so that we can use the results of [25] for the lower bound proof.

Henceforth, let $a \lesssim b$ denote $a \leq Cb$ for a generic positive constant C , not necessarily the same at each occurrence, dependent on the shape regularity of the meshes $\mathcal{S}_h^{n-1,n}$ and d but independent of the space domain Ω , final time T , and the parameters \mathbf{S} , \mathbf{v} , r , f , and u_0 ; C can only depend on the local oscillation of these parameters. Similarly, the notation $a \approx b$ will be employed when simultaneously $a \lesssim b$ and $b \lesssim a$. From now on, we also omit denoting explicitly by (t) the dependence of the estimators on the time. In order to proceed as generally as possible, we will need below the following approximation property of the diffusive flux reconstruction $\boldsymbol{\theta}_h$:

Assumption (C) (Approximation property of the diffusive flux reconstruction)

We suppose that

$$\|\mathbf{S}_h^n \nabla u_h^n + \boldsymbol{\theta}_h^n\|_D \lesssim \left\{ \sum_{\sigma \in \mathcal{G}_D} h_\sigma \|\llbracket \mathbf{S}_h^n \nabla u_h^n \cdot \mathbf{n} \rrbracket\|_\sigma^2 \right\}^{\frac{1}{2}} \quad \forall n \in \{1, \dots, N\}, \forall D \in \mathcal{D}_h^n. \quad (4.16)$$

In (4.16), $\llbracket \cdot \rrbracket$ denotes the jump across a side. Assumption (C) can be shown, in dependence on the construction of $\boldsymbol{\theta}_h^n$ from ∇u_h^n , as in [31].

We also introduce some additional notation. Let $f_h, r_h \in X_h$ and $\mathbf{v}_h \in \mathbf{V}_h$ be space-time discrete approximations of the source term, of the reaction function, and of the velocity field \mathbf{v} , respectively. Let $n \in \{1, \dots, N\}$ and $D \in \mathcal{D}_h^n$. We define the *data oscillation estimator* $\eta_{\text{DO},D}^n$ by

$$\begin{aligned} \eta_{\text{DO},D}^n &:= m_D^n \|f_D^n - f_h^n\|_D + m_D^n \|u_h^n (r_h^n - r_D^n)\|_D \\ &+ \left\{ \sum_{K \in \mathcal{S}_D} \left((m_K^n)^2 \|\nabla \cdot (\mathbf{S} - \mathbf{S}_h^n) \nabla u_{h,\tau}\|_K^2 + \tilde{m}_K^n \sum_{\sigma \in \mathcal{G}_K^{\text{int}}} \|(\mathbf{S} - \mathbf{S}_h^n) \nabla u_{h,\tau} \cdot \mathbf{n}\|_\sigma^2 \right) \right\}^{\frac{1}{2}} \\ &+ \left\{ \sum_{K \in \mathcal{S}_D} \left((m_K^n)^2 \|\nabla \cdot ((\mathbf{v} - \mathbf{v}_h^n) u_{h,\tau})\|_K^2 + \tilde{m}_K^n \sum_{\sigma \in \mathcal{G}_K^{\text{int}}} \|(\mathbf{v} - \mathbf{v}_h^n) u_{h,\tau} \cdot \mathbf{n}\|_\sigma^2 \right) \right\}^{\frac{1}{2}} \end{aligned}$$

and the *quadrature estimator* $\eta_{\text{Q},D}^n$ by

$$\begin{aligned} \eta_{\text{Q},D}^n &:= m_D^n \left\| \frac{u_h^n - u_h^{n-1}}{\tau_n} - \frac{u_D^n - \bar{u}_D^{n-1}}{\tau_n} + r_D^n (u_h^n - u_D^n) - q_D^n \right\|_D \\ &+ \left\{ \sum_{K \in \mathcal{S}_D} \left((m_K^n)^2 \|\nabla \cdot (\mathbf{v}_h^n u_h^n - \mathbf{w}_h^n)\|_K^2 + \tilde{m}_K^n \sum_{\sigma \in \mathcal{G}_K^{\text{int}}} \|(\mathbf{v}_h^n u_h^n - \mathbf{w}_h^n) \cdot \mathbf{n}\|_\sigma^2 \right) \right\}^{\frac{1}{2}}. \end{aligned}$$

We then have the following theorem:

Theorem 4.7 (Efficiency of the a posteriori error estimators in the augmented norm). *Let $\nabla \cdot \mathbf{v} = 0$, let u be the weak solution of problem (1.1a)–(1.1c) given by (2.2) and let $u_{h,\tau} \in X_h$ and $\boldsymbol{\theta}_h, \mathbf{w}_h \in \mathbf{V}_h$ be arbitrary but such that Assumption (C) holds. Let $n \in \{1, \dots, N\}$, let $\mathcal{S}_h^{n-1,n}$ be shape-regular, and let, for all $D \in \mathcal{D}_h^n$, $h_D \approx h_K$ for all $K \in \mathcal{S}_D$. Then*

$$\begin{aligned} (\eta^n)^2 &\lesssim \|u - u_{h,\tau}\|_{Y(t_{n-1}, t_n)}^2 + \int_{t_{n-1}}^{t_n} \sum_{D \in \mathcal{D}_h^n} \{(\eta_{\text{DOQ},D}^n)^2 + (\eta_{\text{DO},D}^n)^2 + (\eta_{\text{Q},D}^n)^2\} dt \\ &+ \|f - f^n - (r - r^n) u_{h,\tau}\|_{X'(t_{n-1}, t_n)}^2. \end{aligned}$$

5 Proof of the a posteriori error estimate and of its efficiency

We shall prove in this section the a posteriori error estimates stated in Theorems 4.1 and 4.2, as well as their efficiency discussed in Theorem 4.7.

5.1 Proof of the a posteriori error estimate

We prove here Theorems 4.1 and 4.2. Let the assumptions of Theorem 4.1 hold.

We start by bounding the error measured in the energy norm (2.3) (and the $L^2(\Omega)$ norm at the end of the simulation) by the residual (and the $L^2(\Omega)$ norm at the beginning of the simulation).

Lemma 5.1 (Bound by the residual). *There holds*

$$\|(u - u_{h,\tau})(\cdot, T)\|^2 + \|u - u_{h,\tau}\|_X^2 \leq \left(\sup_{\varphi \in X, \|\varphi\|_X=1} \int_0^T \langle \mathcal{B}(u - u_{h,\tau}), \varphi \rangle dt \right)^2 + \|(u - u_{h,\tau})(\cdot, 0)\|^2.$$

Proof. Using the obvious relation

$$\int_0^T \langle \mathcal{B}(v), v \rangle dt \leq \sup_{\varphi \in X, \|\varphi\|_X=1} \int_0^T \langle \mathcal{B}(v), \varphi \rangle dt \|v\|_X \leq \frac{1}{2} \left(\sup_{\varphi \in X, \|\varphi\|_X=1} \int_0^T \langle \mathcal{B}(v), \varphi \rangle dt \right)^2 + \frac{1}{2} \|v\|_X^2,$$

valid for any $v \in Z$, the assertion follows from (2.4) and the fact that $(u - u_{h,\tau}) \in Z$. \square

Let from now on, $\varphi \in X$ with $\|\varphi\|_X = 1$ be fixed. Then, on the time interval $(t_{n-1}, t_n]$, $n \in \{1, \dots, N\}$, we have the following results.

We first rewrite the residual $\langle \mathcal{B}(u - u_{h,\tau}), \varphi \rangle$ in a form of a summation whose individual terms will be easy to bound.

Lemma 5.2 (Equivalent form of the residual). *There holds*

$$\langle \mathcal{B}(u - u_{h,\tau}), \varphi \rangle = T_R(\varphi) + T_{\text{DCF}}(\varphi) + T_Q(\varphi)$$

with

$$\begin{aligned} T_R(\varphi) &:= \sum_{D \in \mathcal{D}_h^n} \left(f_D^n - \frac{u_D^n - \bar{u}_D^{n-1}}{\tau_n} - \nabla \cdot \boldsymbol{\theta}_h^n - \nabla \cdot \mathbf{w}_h^n - r_D^n u_D^n - q_D^n, \varphi - \varphi_D \right)_D, \\ T_{\text{DCF}}(\varphi) &:= -(\mathbf{S} \nabla u_{h,\tau} + \boldsymbol{\theta}_h^n - u_{h,\tau} \mathbf{v} + \mathbf{w}_h^n, \nabla \varphi), \\ T_Q(\varphi) &:= \sum_{D \in \mathcal{D}_h^n} \left(f - f_D^n - (u_{h,\tau})_t + \frac{u_D^n - \bar{u}_D^{n-1}}{\tau_n} - r u_{h,\tau} + r_D^n u_D^n + q_D^n, \varphi \right)_D, \end{aligned}$$

where $\varphi_D := (\varphi, 1)_D / |D|$, $D \in \mathcal{D}_h^n$.

Proof. We first use the definition of the weak solution (2.2) and that of \mathcal{B} (2.1) to infer that

$$\langle \mathcal{B}(u - u_{h,\tau}), \varphi \rangle = (f, \varphi) - ((u_{h,\tau})_t, \varphi) - (\mathbf{S} \nabla u_{h,\tau}, \nabla \varphi) - (\nabla \cdot (u_{h,\tau} \mathbf{v}), \varphi) - (r u_{h,\tau}, \varphi).$$

We then add and subtract $(\nabla \cdot \boldsymbol{\theta}_h^n, \varphi)$ and $(\nabla \cdot \mathbf{w}_h^n, \varphi)$ and use the Green theorem to see that

$$\begin{aligned} \langle \mathcal{B}(u - u_{h,\tau}), \varphi \rangle &= (f, \varphi) - ((u_{h,\tau})_t, \varphi) - (\nabla \cdot \boldsymbol{\theta}_h^n, \varphi) - (\nabla \cdot \mathbf{w}_h^n, \varphi) \\ &\quad - (\mathbf{S} \nabla u_{h,\tau} + \boldsymbol{\theta}_h^n - u_{h,\tau} \mathbf{v} + \mathbf{w}_h^n, \nabla \varphi) - (r u_{h,\tau}, \varphi) \\ &= T_R^*(\varphi) + T_{\text{DCF}}(\varphi) + T_Q(\varphi), \end{aligned}$$

where $T_R^*(\varphi)$ is as $T_R(\varphi)$ with, however, the second argument replaced by φ . Finally, it suffices to multiply (4.5) by φ_D , to use therein the Green theorem for the terms involving $\boldsymbol{\theta}_h^n$ and \mathbf{w}_h^n , and add it to $T_R^*(\varphi)$ for each $D \in \mathcal{D}_h^n$ to arrive at the assertion of the lemma. \square

We now bound separately the three terms of Lemma 5.2.

Lemma 5.3 (Residual estimate). *There holds*

$$T_R(\varphi) \leq \sum_{D \in \mathcal{D}_h^n} \eta_{R,D}^n \|\varphi\|_D.$$

Proof. The assertion follows immediately from an application of the Cauchy–Schwarz inequality, the Poincaré inequality (4.1), and the definition (2.3) of the energy norm $\|\cdot\|$, cf. [30, Lemmas 4.3 and 7.1]. \square

Lemma 5.4 (Diffusive and convective flux estimates). *There holds*

$$T_{\text{DCF}}(\varphi) \leq \sum_{D \in \mathcal{D}_h^n} \eta_{\text{DCF},D}^n \|\varphi\|_D, \quad (5.1a)$$

$$T_{\text{DCF}}(\varphi) \leq \left\{ \sum_{D \in \mathcal{D}_h^n} (\eta_{\text{DF},D}^n)^2 \right\}^{\frac{1}{2}} \|\varphi\| + \sup_{\psi \in H_0^1(\Omega); \|\psi\|=1} (\nabla \cdot (u_{h,\tau} \mathbf{v} - \mathbf{w}_h^n), \psi) \|\varphi\|. \quad (5.1b)$$

Proof. Estimate (5.1a) follows easily by the Cauchy–Schwarz inequality and (2.3). The first part of estimate (5.1b), bounding the term $-(\mathbf{S} \nabla u_{h,\tau} + \boldsymbol{\theta}_h^n, \nabla \varphi)$, is established as in [7, proof of Theorem 4.4]. Two following simple modifications are necessary: firstly, the Friedrichs inequality (4.2) has to be used for $K \in \mathcal{S}_h^{n-1,n,\text{ext}}$ instead of the Poincaré inequality (4.1) in [7, proof of Theorem 4.4]; consequently, only a sum over the sides of the elements K not contained in $\partial\Omega$, $\sigma \in \mathcal{G}_K^{\text{int}}$, and not a sum over all sides of the elements K , $\sigma \in \mathcal{G}_K$, appears in the definition (4.11) of $\eta_{\text{DF},D}^n$. Secondly, the scaling by \mathbf{S} has to be added, leading to the factors $c_{\mathbf{S},K}^n$ in the definitions (4.10a)–(4.10b) of m_K^n and \tilde{m}_K^n . Finally, by the Green theorem, we easily have

$$(u_{h,\tau} \mathbf{v} - \mathbf{w}_h^n, \nabla \varphi) = -(\nabla \cdot (u_{h,\tau} \mathbf{v} - \mathbf{w}_h^n), \varphi) \leq \sup_{\psi \in H_0^1(\Omega); \|\psi\|=1} (\nabla \cdot (u_{h,\tau} \mathbf{v} - \mathbf{w}_h^n), \psi) \|\varphi\|.$$

\square

Lemma 5.5 (Data oscillation–quadrature estimate). *There holds*

$$T_Q(\varphi) \leq \left\{ \sum_{D \in \mathcal{D}_h^n} (\eta_{\text{DOQ},D}^n)^2 \right\}^{\frac{1}{2}} \|\varphi\|.$$

Proof. Denote by v_D the argument in the left part of $(\cdot, \cdot)_D$ in $T_Q(\varphi)$ in Lemma 5.2. Then, on the one hand,

$$T_Q(\varphi) \leq \sum_{D \in \mathcal{D}_h^n} \|v_D\|_D \|\varphi\|_D \leq \sum_{D \in \mathcal{D}_h^n} (c_{\mathbf{v},r,D}^n)^{-\frac{1}{2}} \|v_D\|_D \|\varphi\|_D \leq (c_{\mathbf{v},r,\Omega}^n)^{-\frac{1}{2}} \left\{ \sum_{D \in \mathcal{D}_h^n} \|v_D\|_D^2 \right\}^{\frac{1}{2}} \|\varphi\|$$

by the Cauchy–Schwarz inequality and definition (2.3) of the energy norm. On the other hand,

$$T_Q(\varphi) \leq \left\{ \sum_{D \in \mathcal{D}_h^n} \|v_D\|_D^2 \right\}^{\frac{1}{2}} \|\varphi\| \leq C_F^{\frac{1}{2}} h_\Omega (c_{\mathbf{S},\Omega}^n)^{-\frac{1}{2}} \left\{ \sum_{D \in \mathcal{D}_h^n} \|v_D\|_D^2 \right\}^{\frac{1}{2}} \|\varphi\|$$

by the Cauchy–Schwarz inequality, the Friedrichs inequality (4.3), and definition (2.3) of the energy norm. \square

We are now ready to prove Theorem 4.1.

Proof of Theorem 4.1. Let $\varphi \in X$, $\|\varphi\|_X = 1$, be fixed. Lemmas 5.2–5.5 and the Cauchy–Schwarz inequality imply

$$\langle \mathcal{B}(u - u_{h,\tau}), \varphi \rangle dt \leq \left(\left\{ \sum_{D \in \mathcal{D}_h^n} (\eta_{\mathbb{R},D}^n + \eta_{\text{DCF},D}^n)^2 \right\}^{\frac{1}{2}} + \left\{ \sum_{D \in \mathcal{D}_h^n} (\eta_{\text{DOQ},D}^n)^2 \right\}^{\frac{1}{2}} \right) \|\varphi\|,$$

using the bound (5.1a) on $T_{\text{DCF}}(\varphi)$. Similarly, using the bound (5.1b) on $T_{\text{DCF}}(\varphi)$, we arrive at

$$\begin{aligned} \langle \mathcal{B}(u - u_{h,\tau}), \varphi \rangle dt \leq & \left(\left\{ \sum_{D \in \mathcal{D}_h^n} (\eta_{\mathbb{R},D}^n)^2 \right\}^{\frac{1}{2}} + \left\{ \sum_{D \in \mathcal{D}_h^n} (\eta_{\text{DF},D}^n)^2 \right\}^{\frac{1}{2}} \right. \\ & \left. + \sup_{\psi \in H_0^1(\Omega); \|\psi\|=1} (\nabla \cdot (u_{h,\tau} \mathbf{v} - \mathbf{w}_h^n), \psi) + \left\{ \sum_{D \in \mathcal{D}_h^n} (\eta_{\text{DOQ},D}^n)^2 \right\}^{\frac{1}{2}} \right) \|\varphi\|. \end{aligned}$$

Another use of the Cauchy–Schwarz inequality gives

$$\int_0^T \langle \mathcal{B}(u - u_{h,\tau}), \varphi \rangle dt \leq \sum_{n=1}^N \left(\min\{\eta^{(1),n}, \eta^{(2),n}\} \left\{ \int_{t_{n-1}}^{t_n} \|\varphi\|^2 dt \right\}^{\frac{1}{2}} \right) \leq \eta \|\varphi\|_X = \eta \quad (5.2)$$

and using Lemma 5.1 concludes the proof. \square

Along the same rules as above, we now also prove Theorem 4.2.

Proof of Theorem 4.2. Let us first bound the term $\|\partial_t(u - u_{h,\tau}) + b_A(u - u_{h,\tau})\|_{X'}^2$, stemming from the definition (2.7) of the augmented norm. Following [10, 11], using definitions (2.1) and (2.6), estimate (5.2), and the Cauchy–Schwarz inequality, we readily have

$$\begin{aligned} & \sup_{\varphi \in X; \|\varphi\|_X=1} \int_0^T \langle \partial_t(u - u_{h,\tau}) + b_A(u - u_{h,\tau}), \varphi \rangle(t) dt \\ &= \sup_{\varphi \in X; \|\varphi\|_X=1} \int_0^T \{ \langle \mathcal{B}(u - u_{h,\tau}), \varphi \rangle - \langle \mathcal{B}_S(u - u_{h,\tau}), \varphi \rangle \}(t) dt \\ &\leq \eta + \|u - u_{h,\tau}\|_X. \end{aligned}$$

Consequently, using Theorem 4.1,

$$\|\partial_t(u - u_{h,\tau}) + b_A(u - u_{h,\tau})\|_{X'}^2 \leq 4\eta^2 + 2\|(u - u_{h,\tau})(\cdot, 0)\|^2 - 2\|(u - u_{h,\tau})(\cdot, T)\|^2.$$

The assertion of the theorem follows from definition (2.7) of the augmented norm. \square

5.2 Proof of the efficiency of the estimate

We prove here Theorem 4.7. Let its assumptions hold. Let first $n \in \{1, \dots, N\}$ and $K \in \mathcal{S}_h^{n-1,n}$ be fixed. We denote by

$$\begin{aligned} \eta_{\mathbb{R},K}^n &:= m_K^n \left\| f_h^n - \frac{u_h^n - u_h^{n-1}}{\tau_n} + \nabla \cdot (\mathbf{S}_h^n \nabla u_h^n) - \nabla \cdot (\mathbf{v}_h^n u_h^n) - r_h^n u_h^n \right\|_K, \\ \eta_{\mathbb{J},K}^n &:= (m_K^n)^{\frac{1}{2}} (c_{\mathbf{S},K}^n)^{-\frac{1}{4}} \sum_{\sigma \in \mathcal{G}_K^{\text{int}}} \| [\mathbf{S}_h^n \nabla u_h^n \cdot \mathbf{n}] \|_{\sigma}, \end{aligned}$$

respectively, the usual element and face residual estimators, cf. [25]. In order to prove Theorem 4.7, we show in the following lemmas that our a posteriori error estimate represents a lower bound for the residual a posteriori error estimate of [25, Lemma 7.1]. Consequently, we will be able to establish the lower bound by estimate (7.2) of this reference.

Let $n \in \{1, \dots, N\}$ and $D \in \mathcal{D}_h^n$ be fixed. We then have the following results:

Lemma 5.6 (Upper bound on $\eta_{\mathbf{R},D}^n$). *There holds*

$$\eta_{\mathbf{R},D}^n \lesssim \left\{ \sum_{K \in \mathcal{S}_D} (\eta_{\mathbf{R},K}^n)^2 \right\}^{\frac{1}{2}} + \left\{ \sum_{K \in \mathcal{S}_D} (\eta_{\mathbf{J},K}^n)^2 \right\}^{\frac{1}{2}} + \eta_{\text{DO},D}^n + \eta_{\mathbf{Q},D}^n.$$

Proof. The triangle inequality yields

$$\begin{aligned} \eta_{\mathbf{R},D}^n &\leq m_D^n \left\| f_h^n - \frac{u_h^n - u_h^{n-1}}{\tau_n} + \nabla \cdot (\mathbf{S}_h^n \nabla u_h^n) - \nabla \cdot (\mathbf{v}_h^n u_h^n) - r_h^n u_h^n \right\|_D + m_D^n \|f_D^n - f_h^n\|_D \\ &\quad + m_D^n \left\| \frac{u_h^n - u_h^{n-1}}{\tau_n} - \frac{u_D^n - \bar{u}_D^{n-1}}{\tau_n} + r_D^n (u_h^n - u_D^n) - q_D^n \right\|_D \\ &\quad + m_D^n \|u_h^n (r_h^n - r_D^n)\|_D + m_D^n \|\nabla \cdot (\mathbf{S}_h^n \nabla u_h^n + \boldsymbol{\theta}_h^n)\|_D + m_D^n \|\nabla \cdot (\mathbf{v}_h^n u_h^n - \mathbf{w}_h^n)\|_D. \end{aligned}$$

The fact that $\mathbf{S}_h^n \nabla u_h^n + \boldsymbol{\theta}_h^n$ is a piecewise polynomial in D , the inverse inequality, the fact that $h_D \approx h_K$ for all $K \in \mathcal{S}_D$, and the approximation property (4.16) lead to

$$\|\nabla \cdot (\mathbf{S}_h^n \nabla u_h^n + \boldsymbol{\theta}_h^n)\|_D \lesssim h_D^{-1} \|\mathbf{S}_h^n \nabla u_h^n + \boldsymbol{\theta}_h^n\|_D \lesssim h_D^{-1} \left\{ \sum_{\sigma \in \mathcal{G}_D} h_\sigma \|\llbracket \mathbf{S}_h^n \nabla u_h^n \cdot \mathbf{n} \rrbracket_\sigma^2 \right\}^{\frac{1}{2}}.$$

From here, we easily get

$$m_D \|\nabla \cdot (\mathbf{S}_h^n \nabla u_h^n + \boldsymbol{\theta}_h^n)\|_D \lesssim \left\{ \sum_{K \in \mathcal{S}_D} (\eta_{\mathbf{J},K}^n)^2 \right\}^{\frac{1}{2}},$$

using the previous arguments and the bound $m_K^n h_K^{-\frac{1}{2}} \lesssim (m_K^n)^{\frac{1}{2}} (c_{\mathbf{S},K}^n)^{-\frac{1}{4}}$ (equivalent to the obvious $(m_K^n)^{\frac{1}{2}} h_K^{-\frac{1}{2}} (c_{\mathbf{S},K}^n)^{\frac{1}{4}} \lesssim 1$) in each $K \in \mathcal{S}_D$. Combining the above results, the assertion follows. \square

Lemma 5.7 (Upper bound on $\eta_{\text{DF},D}^n$). *There holds*

$$\eta_{\text{DF},D}^n \lesssim \left\{ \sum_{K \in \mathcal{S}_D} (\eta_{\mathbf{J},K}^n)^2 \right\}^{\frac{1}{2}} + \left\{ \sum_{K \in \mathcal{S}_D} m_K^n (c_{\mathbf{S},K}^n)^{-\frac{1}{2}} h_K^{-1} \|\mathbf{S}_h^n \nabla (u_{h,\tau} - u_h^n)\|_K^2 \right\}^{\frac{1}{2}} + \eta_{\text{DO},D}^n.$$

Proof. Let $K \in \mathcal{S}_D$. We have, separating the data oscillation, time evolution, and diffusive flux

approximation parts,

$$\begin{aligned}
& m_K^n \|\nabla \cdot (\mathbf{S} \nabla u_{h,\tau} + \boldsymbol{\theta}_h^n)\|_K + (\tilde{m}_K^n)^{\frac{1}{2}} \sum_{\sigma \in \mathcal{G}_K^{\text{int}}} (C_{t,K,\sigma})^{\frac{1}{2}} \|(\mathbf{S} \nabla u_{h,\tau} + \boldsymbol{\theta}_h^n) \cdot \mathbf{n}\|_\sigma \\
& \lesssim m_K^n \|\nabla \cdot (\mathbf{S} \nabla u_{h,\tau} + \boldsymbol{\theta}_h^n)\|_K + (\tilde{m}_K^n)^{\frac{1}{2}} \sum_{\sigma \in \mathcal{G}_K^{\text{int}}} \|(\mathbf{S} \nabla u_{h,\tau} + \boldsymbol{\theta}_h^n) \cdot \mathbf{n}\|_\sigma \\
& \leq m_K^n (\|\nabla \cdot (\mathbf{S} - \mathbf{S}_h^n) \nabla u_{h,\tau}\|_K + \|\nabla \cdot \mathbf{S}_h^n \nabla (u_{h,\tau} - u_h^n)\|_K + \|\nabla \cdot (\mathbf{S}_h^n \nabla u_h^n + \boldsymbol{\theta}_h^n)\|_K) \\
& \quad + (\tilde{m}_K^n)^{\frac{1}{2}} \sum_{\sigma \in \mathcal{G}_K^{\text{int}}} (\|(\mathbf{S} - \mathbf{S}_h^n) \nabla u_{h,\tau} \cdot \mathbf{n}\|_\sigma + \|\mathbf{S}_h^n \nabla (u_{h,\tau} - u_h^n) \cdot \mathbf{n}\|_\sigma + \|(\mathbf{S}_h^n \nabla u_h^n + \boldsymbol{\theta}_h^n) \cdot \mathbf{n}\|_\sigma) \\
& \lesssim m_K^n \|\nabla \cdot (\mathbf{S} - \mathbf{S}_h^n) \nabla u_{h,\tau}\|_K + (\tilde{m}_K^n)^{\frac{1}{2}} \sum_{\sigma \in \mathcal{G}_K^{\text{int}}} \|(\mathbf{S} - \mathbf{S}_h^n) \nabla u_{h,\tau} \cdot \mathbf{n}\|_\sigma \\
& \quad + (m_K^n)^{\frac{1}{2}} (c_{\mathbf{S},K}^n)^{-\frac{1}{4}} h_K^{-\frac{1}{2}} (\|\mathbf{S}_h^n \nabla (u_{h,\tau} - u_h^n)\|_K + \|\mathbf{S}_h^n \nabla u_h^n + \boldsymbol{\theta}_h^n\|_K),
\end{aligned}$$

using the inverse inequalities

$$\begin{aligned}
\|\nabla \cdot \mathbf{q}_h\|_K & \lesssim h_K^{-1} \|\mathbf{q}_h\|_K, \\
\|\mathbf{q}_h \cdot \mathbf{n}\|_\sigma & \lesssim h_K^{-\frac{1}{2}} \|\mathbf{q}_h\|_K
\end{aligned}$$

for $\mathbf{q}_h = \mathbf{S}_h^n \nabla (u_{h,\tau} - u_h^n)$ and $\mathbf{q}_h = \mathbf{S}_h^n \nabla u_h^n + \boldsymbol{\theta}_h^n$ and the estimate

$$m_K^n h_K^{-\frac{1}{2}} + (\tilde{m}_K^n)^{\frac{1}{2}} \lesssim (m_K^n)^{\frac{1}{2}} (c_{\mathbf{S},K}^n)^{-\frac{1}{4}}$$

following from [7, Proof of Theorem 5.1]. To conclude, it now suffices to use the Cauchy–Schwarz inequality, approximation property (4.16), and the definitions of $\eta_{J,K}^n$ and $\eta_{\text{DO},D}^n$. \square

Let $n \in \{1, \dots, N\}$ and $K \in \mathcal{S}_h^{n-1,n}$ be fixed. We then have:

Lemma 5.8 (Equivalent form of $\int_{t_{n-1}}^{t_n} \|\mathbf{S}_h^n \nabla (u_{h,\tau} - u_h^n)\|_K^2 dt$). *There holds*

$$\int_{t_{n-1}}^{t_n} \|\mathbf{S}_h^n \nabla (u_{h,\tau} - u_h^n)\|_K^2 dt = \frac{\tau_n}{3} \|\mathbf{S}_h^n \nabla (u_h^n - u_h^{n-1})\|_K^2.$$

Proof. Follows from the definition of $u_{h,\tau}$ by (3.9), cf. [24, Equation (6.5)]. \square

Let $n \in \{1, \dots, N\}$ be fixed. We then have:

Lemma 5.9 (Upper bound on the convective time evolution term). *There holds*

$$\begin{aligned}
\int_{t_{n-1}}^{t_n} \left(\sup_{\varphi \in H_0^1(\Omega); \|\varphi\|=1} (\nabla \cdot (u_{h,\tau} \mathbf{v} - \mathbf{w}_h^n), \varphi) \right)^2 dt & \lesssim \tau_n \sup_{\varphi \in H_0^1(\Omega); \|\varphi\|=1} (\nabla \cdot ((u_h^n - u_h^{n-1}) \mathbf{v}_h^n), \varphi)^2 \\
& \quad + \int_{t_{n-1}}^{t_n} \sum_{D \in \mathcal{D}_h^n} \{(\eta_{\text{DO},D}^n)^2 + (\eta_{\text{Q},D}^n)^2\} dt.
\end{aligned}$$

Proof. Let $t \in (t_{n-1}, t_n]$ and $\varphi \in H_0^1(\Omega)$. Then, separating the data oscillation, time evolution, and quadrature parts,

$$\begin{aligned}
(\nabla \cdot (u_{h,\tau} \mathbf{v} - \mathbf{w}_h^n), \varphi) & = (\nabla \cdot (u_{h,\tau} (\mathbf{v} - \mathbf{v}_h^n)), \varphi) + (\nabla \cdot ((u_{h,\tau} - u_h^n) \mathbf{v}_h^n), \varphi) + (\nabla \cdot (u_h^n \mathbf{v}_h^n - \mathbf{w}_h^n), \varphi) \\
& = -(u_{h,\tau} (\mathbf{v} - \mathbf{v}_h^n), \nabla \varphi) + (\nabla \cdot ((u_{h,\tau} - u_h^n) \mathbf{v}_h^n), \varphi) - (u_h^n \mathbf{v}_h^n - \mathbf{w}_h^n, \nabla \varphi)
\end{aligned}$$

Bounding the first and last terms of the above expression as in (5.1b) in Lemma 5.4 and integrating the middle term in time as in Lemma 5.8, the assertion of the lemma follows. \square

With the above developments, we can now bound our estimators by the classical residual ones.

Lemma 5.10 (Upper bound on $(\eta^n)^2$ using the usual residual estimators). *There holds*

$$\begin{aligned}
(\eta^n)^2 &\leq (\eta^{(2),n})^2 \lesssim \tau_n \sum_{D \in \mathcal{D}_h^n} \sum_{K \in \mathcal{S}_D} \{(\eta_{R,K}^n)^2 + (\eta_{J,K}^n)^2 + (c_{\mathbf{S},K}^n)^{-1} \|\mathbf{S}_h^n \nabla(u_h^n - u_h^{n-1})\|_K^2\} \\
&+ \int_{t_{n-1}}^{t_n} \sum_{D \in \mathcal{D}_h^n} \{(\eta_{\text{DOQ},D}^n)^2 + (\eta_{\text{DO},D}^n)^2 + (\eta_{\text{Q},D}^n)^2\} dt \\
&+ \tau_n \sup_{\varphi \in H_0^1(\Omega); \|\varphi\|=1} (\nabla \cdot ((u_h^n - u_h^{n-1}) \mathbf{v}_h^n), \varphi)^2.
\end{aligned}$$

Proof. Follows by combining the results of Lemmas 5.6–5.9. □

We are now ready to announce the main result of this section.

Proof of Theorem 4.7. Follows by combining Lemma 5.10 and [25, Lemma 7.1]. □

6 Adaptive algorithm

We present here an adaptive algorithm based on our a posteriori error estimates which is designed to ensure that the relative energy error between the exact and approximate solutions will be below a prescribed tolerance ε . Recalling Corollary (4.6), we impose that

$$\frac{\sum_{n=1}^N (\eta_{\text{sp}}^n + \eta_{\text{tm}}^n)^2}{\sum_{n=1}^N \|u_{h,\tau}\|_{X(t_{n-1}, t_n)}^2} \leq \varepsilon^2. \tag{6.1}$$

On a given time level t_{n-1} , we in particular choose the space mesh \mathcal{D}_h^n and time step τ_n such that

$$\eta_{\text{sp}}^n \leq \varepsilon \frac{\|u_{h,\tau}\|_{X(t_{n-1}, t_n)}}{2}, \quad \eta_{\text{tm}}^n \leq \varepsilon \frac{\|u_{h,\tau}\|_{X(t_{n-1}, t_n)}}{2}.$$

At the same time, using the fact that there are no unknown constants hidden in both η_{sp}^n and η_{tm}^n , we intend to equilibrate the space and time estimators η_{sp}^n and η_{tm}^n , in the hope to equilibrate the space and time contributions to the error.

For practical implementation purposes, we introduce the maximal refinement level parameters N_{sp} and N_{tm} . Altogether with some other parameters of the algorithm, they are listed in Table 1. We also denote by **SpTmUnkn** the total number of space–time unknowns. The actual algorithm is as follows:

- let an initial mesh \mathcal{D}_h^0 and an initial time step τ_1 be given
- set up the initial conditions on \mathcal{D}_h^0
- set $t_0 = t_1 = 0$, $\mathcal{D}_h^1 = \mathcal{D}_h^0$, and $n = 1$
- set **EstSpPrev** = 1, **EstTmPrev** = 0
- set **LevTmRef** = 0, **SpTmUnkn** = 0
- set $\eta = 0$
- while** $t_n < T$
 - set **Count** = 0
 - set $t_n = t_{n-1} + \tau_n$
 - set up the boundary conditions on \mathcal{D}_h^n
 - set $\eta_{\text{sp}}^n = \mathbf{Crit} = 1$, **ItSpRef** = 1

Parameter	Meaning
N_{sp}	maximal level of space refinement
N_{tm}	maximal level of time refinement
Ref	percentage of cells for the space mesh refinement
Deref	percentage of cells for the space mesh derefinement
Bulk	spatial error estimate fraction for the derefinement
DerefSp	error estimate percentage for the space mesh derefinement
DerefTm	error estimate percentage for the time mesh derefinement
Comp	parameter for comparison of η_{sp} and η_{tm}
StepsSpDeref	number of steps after which the space mesh is derefined
StepsTmDeref	number of steps after which the time mesh is derefined

Table 1: Different parameters of the adaptive algorithm and their meaning

- **while** $\eta_{\text{sp}}^n \geq \text{Crit}$, $\text{ItSpRef} \leq N_{\text{sp}} + 1$, and $\text{EstSpPrev} > \text{Comp} \cdot \text{EstTmPrev}$ when $\text{ItSpRef} \neq 1$
 - **if** $\text{ItSpRef} > 1$
 - refine such cells $D \in \mathcal{D}_h^n$ where $\eta_{D,\text{sp}}^n \geq \text{Ref} \cdot \max_{E \in \mathcal{D}_h^n} \eta_{E,\text{sp}}^n$ and such that their level of refinement is less than N_{sp}
 - create a new mesh \mathcal{D}_h^n and interpolate the data onto this new mesh
 - solve (3.1) on \mathcal{D}_h^n with the time step τ_n to get new $u_{h,\tau}|_{[t_{n-1}, t_n]}$
 - compute the space a posteriori error estimate η_{sp}^n
 - set $\text{EstSpPrev} = \eta_{\text{sp}}^n / \sqrt{\tau_n}$
 - compute the norm of the approximate solution $\|u_{h,\tau}\|_{X(t_{n-1}, t_n)}$ and set $\text{Crit} = \varepsilon \cdot \|u_{h,\tau}\|_{X(t_{n-1}, t_n)} / 2$
 - set $\text{ItSpRef} = \text{ItSpRef} + 1$
- compute the time a posteriori error estimate η_{tm}^n
- set $\text{EstTmPrev} = \eta_{\text{tm}}^n / \sqrt{\tau_n}$
- **if** $\eta_{\text{tm}}^n \geq \text{Crit}$, $\text{LevTmRef} < N_{\text{tm}}$, and $\text{EstTmPrev} > \text{Comp} \cdot \text{EstSpPrev}$
 - set $t_n = t_n - \tau_n$, $\tau_n = \tau_n / 3$, and $\text{LevTmRef} = \text{LevTmRef} + 1$
- **else**
 - $\eta^2 = \eta^2 + (\eta_{\text{tm}}^n + \eta_{\text{sp}}^n)^2$
 - $\text{SpTmUnkn} = \text{SpTmUnkn} + |\mathcal{D}_h^n|$
 - $\text{Count} = \text{Count} + 1$
 - **if** Count is a multiple of StepsSpDeref
 - set NBulkCells as the number of cells which contain $\text{Bulk} \cdot \text{EstSpPrev}$ part of the spatial error
 - derefine such cells $D \in \mathcal{D}_h^n$ that $\eta_{D,\text{sp}}^n \leq \text{Deref} \cdot \max_{E \in \mathcal{D}_h^n} \eta_{E,\text{sp}}^n$ and that $\eta_{D,\text{sp}}^n < \text{Comp} \cdot \text{DerefSp} \cdot \text{EstTmPrev} \cdot \sqrt{\tau_n} / 2 / \text{NBulkCells}$
 - create a new mesh \mathcal{D}_h^n and interpolate the data onto this mesh
 - **if** Count is a multiple of StepsTmDeref and $\text{EstTmPrev} < \text{Comp} \cdot \text{DerefTm} \cdot \text{EstSpPrev}$, set $\tau_n = 3\tau_n$ and $\text{LevTmRef} = \text{LevTmRef} - 1$
 - set $\mathcal{D}_h^{n+1} = \mathcal{D}_h^n$, $\tau_{n+1} = \tau_n$, and $n = n + 1$

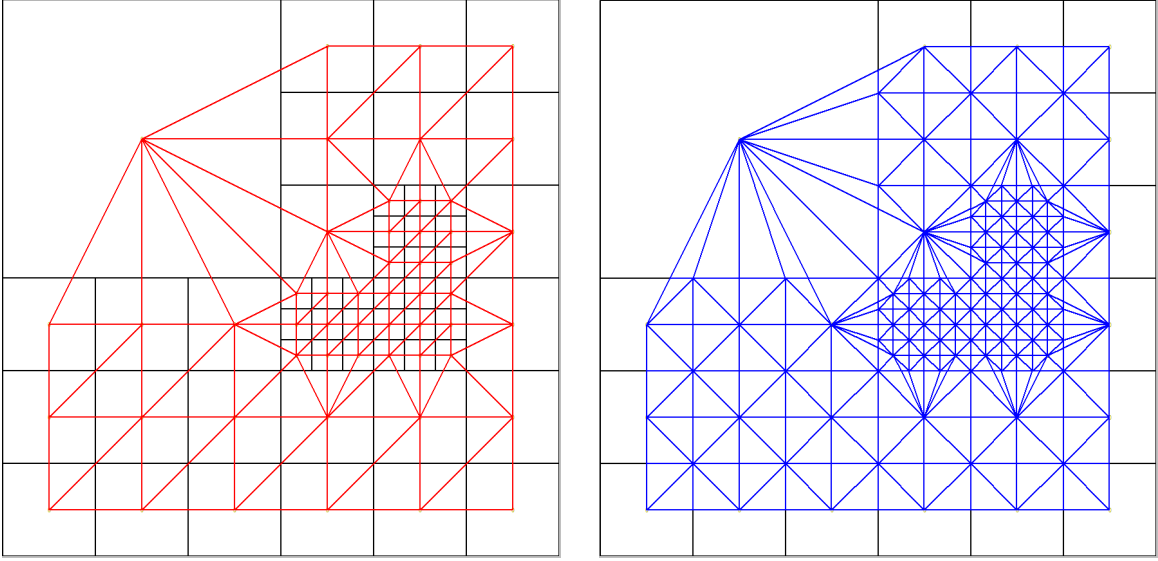


Figure 2: Nonmatching primal square mesh \mathcal{D}_h^n , the corresponding dual triangular mesh \mathcal{T}_h^n (in red, left), and the corresponding tertial triangular mesh $\mathcal{S}_h^{n-1,n}$ (in blue, right)

7 Numerical experiments

We apply in this section the a posteriori error estimates of Theorem 4.1 and the adaptive algorithm of Section 6 to a model problem with a known analytic solution.

We consider (1.1a)–(1.1c) with

$$\begin{aligned}\Omega &= (0, 3) \times (0, 3), \\ \mathbf{S} &= \nu \begin{pmatrix} 1 & 0 \\ 0 & 1 \end{pmatrix}, \\ \mathbf{v} &= (v_1, v_2), \\ r &= 0, \\ f &= 0,\end{aligned}$$

where $v_1 = 0.8$ and $v_2 = 0.4$ are two constant components of the convective field \mathbf{v} and the parameter $\nu > 0$ determines the amount of diffusion. We will consider the cases $\nu = 0.001$ and $\nu = 10$. The initial condition u_0 , as well as the (inhomogeneous) Dirichlet boundary condition, are given by the exact solution

$$u(x, y, t) = \frac{1}{200\nu(t + t_0) + 1} e^{-50 \frac{(x-x_0-v_1(t+t_0))^2 + (y-y_0-v_2(t+t_0))^2}{200\nu(t+t_0)+1}}.$$

This solution represents a Gaussian peak centered at the point (x_0, y_0) at time $t = 0$, moved through the domain Ω by the convective field \mathbf{v} , and diffusing with the intensity given by the parameter ν . We use in particular $x_0 = 0.5$ and $y_0 = 1.35$. Unless otherwise specified, we set the additional nonnegative parameter t_0 to $t_0 = 0$. We will test two cases with the final time $T = 0.6$ and $T = 1.5$, respectively.

We consider the scheme (3.1) on square meshes with possibly nonmatching refinements as indicated in Figure 2. Recall that the diffusive and convective flux reconstructions $\boldsymbol{\theta}_h$ and \mathbf{w}_h are constructed in the space \mathbf{V}_h ; for each time level t_n , they are Raviart–Thomas–Nédélec vector fields

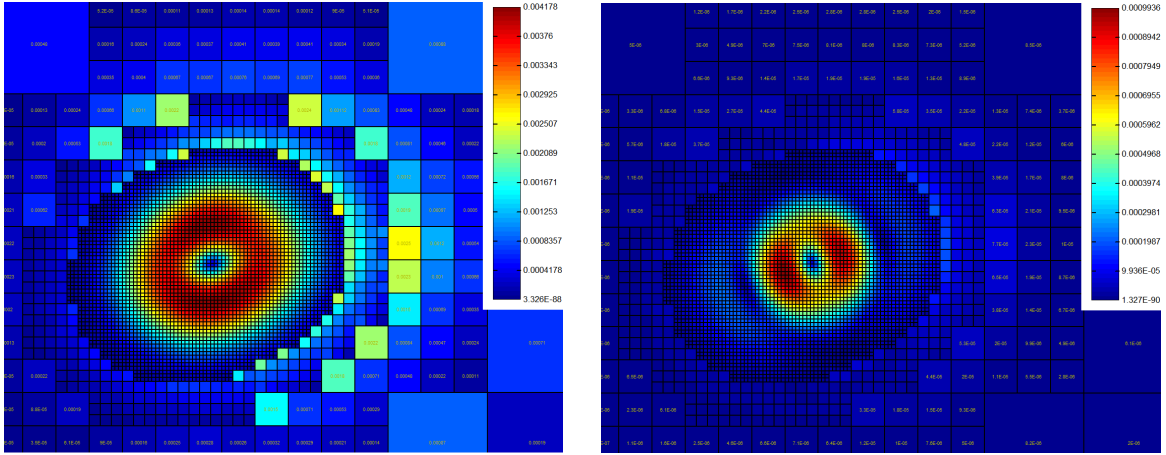


Figure 3: Estimated (left) and actual (right) energy error distribution, adaptive refinement, $\nu = 0.001$, $T = 0.6$, adaptively refined mesh with $N_{\text{sp}} = N_{\text{tm}} = 4$

over the fine simplicial meshes $\mathcal{S}_h^{n-1,n}$ (cf. the right part of Figure 2). Their degrees of freedom (normal fluxes) over the boundaries of the elements D of the grid \mathcal{D}_h^n are defined respectively by (4.6) and (4.7). The remaining degrees of freedom are fixed as $\mathbf{t}_{2,D}$ in [31, Section 4.3.3]. By such a construction, in particular, the residual estimators (4.8) all vanish. We present the results of Theorem 4.1 in the energy norm (2.3) setting; we use the estimator η given by (4.13b), where we only evaluate $\eta^{(1),n}$. We do not present the results of Theorem 4.2 for the augmented norm (2.7) since this norm is not easily calculable and since we have decided not to evaluate/compute the upper bound on the estimator $\eta^{(2),n}$, see Remark 4.4. We neglect the additional error from the inhomogeneous Dirichlet boundary condition.

The starting mesh \mathcal{D}_h^1 is given by a uniform 10×10 space grid and a uniform division of the time interval into 2 time steps when $T = 0.6$ and 5 time steps when $T = 1.5$. The meshes \mathcal{D}_h^n are refined either uniformly or adaptively. In the first case, each square is always divided into nine subsquares, and the time step is cut by three. In the second case, the adaptive algorithm proposed in Section 6 is employed. We set $\text{Ref} = 0.5$, $\text{Deref} = 0.05$, $\text{Comp} = 0.7$, $\text{StepsSpDeref} = 6$, $\text{StepsTmDeref} = 6$, $\text{Bulk} = 0.85$, $\text{DerefSp} = 0.15$, and $\text{DerefTm} = 0.5$. We will be choosing different values of N_{sp} and N_{tm} (recall their definition in Table 1). As we limit the maximal level of space and time refinements, we usually do not achieve the prescribed tolerance ε in (6.1). Finally, we define the experimental order of convergence ξ by

$$\xi := \frac{\log(e_N) - \log(e_{N-1})}{\frac{1}{3} \log |\mathcal{V}_{N-1}| - \frac{1}{3} \log |\mathcal{V}_N|},$$

where e_N is the error on the last space–time mesh, e_{N-1} is the error on the last but one space–time mesh, and $|\mathcal{V}_N|$ and $|\mathcal{V}_{N-1}|$ denote the corresponding numbers of total space–time unknowns given by $\sum_{n=1}^N |\mathcal{D}_h^n|$.

7.1 Overall performance

We first consider $\nu = 0.001$ and $T = 0.6$. In this case, the problem is strongly convection-dominated with a very small amount of diffusion; the initial maximal value is 1, whereas the maximal value at the end of the simulation is roughly 0.9. Figure 9 below shows some approximate solutions. In Figure 3, we compare the actual error distribution and the one predicted by our a

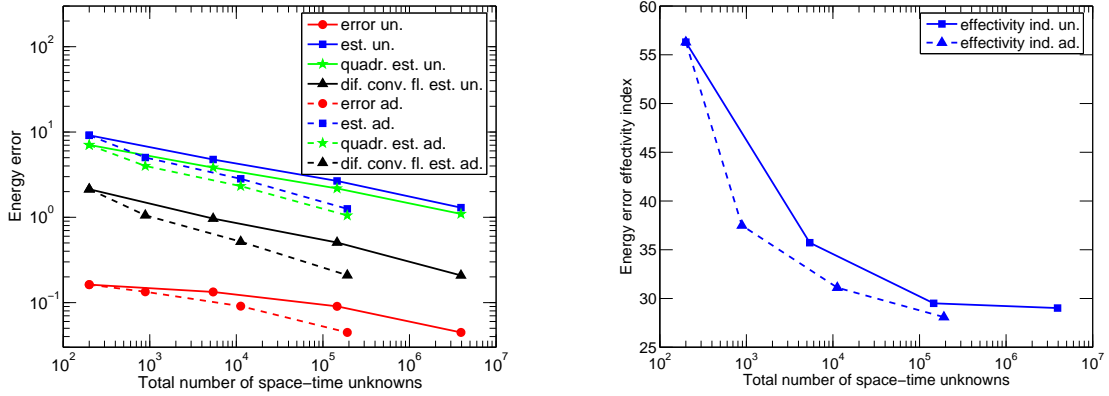


Figure 4: Estimated and actual energy errors (left) and corresponding effectivity indices (right), $\nu = 0.001$, $T = 0.6$

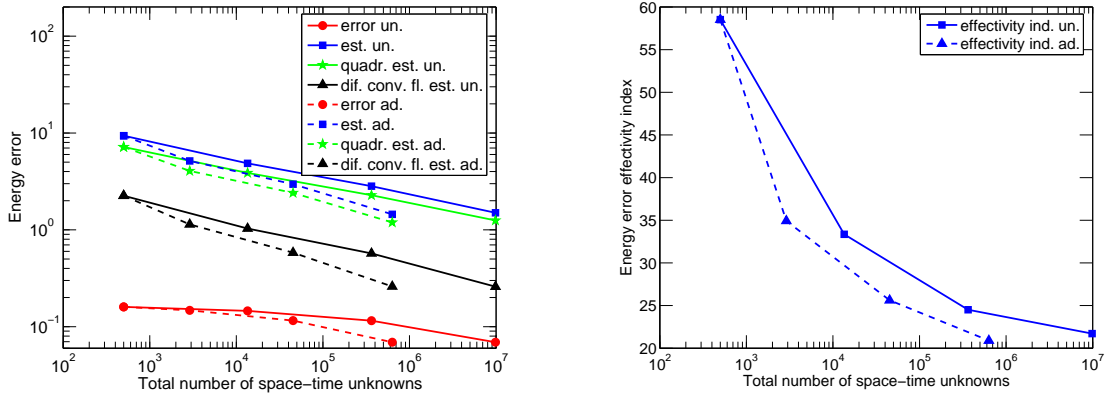


Figure 5: Estimated and actual energy errors (left) and corresponding effectivity indices (right), $\nu = 0.001$, $T = 1.5$

posteriori error estimate. The result is presented at the final time, on an adaptively refined mesh with $N_{\text{sp}} = N_{\text{tm}} = 4$. We can see that a correct form of the error distribution is predicted (circular with smaller error in the middle of the circle), whereas this is not completely the case for the localization—the predicted error distribution is [—] more spread. We anticipate that this is caused by the fact that the solution itself is rather diffused; increasing N_{sp} and N_{tm} improves this considerably.

We next, in the left part of Figure 4, compare the actual error ($\|(u - u_{h,\tau})(\cdot, T)\|^2 + \|u - u_{h,\tau}\|_X^2\|_X^2)^{\frac{1}{2}}$ with the estimate $(\eta^2 + \|u_0 - u_{h,\tau}(\cdot, 0)\|^2)^{\frac{1}{2}}$ on uniformly/adaptively refined meshes. In the right part of Figure 4, we present the corresponding effectivity indices, given as the ratios of the estimate over the error. In the adaptive refinement strategy, we obtain the same precision for much fewer (roughly 20 times less for the last meshes) space-time unknowns than in the uniform one. Concerning the experimental order of convergence, we have found $\xi = 0.64$ and $\xi = 0.75$ in the uniform and adaptive cases, respectively. The effectivity indices depend on the local Péclet number and improve as the mesh is refined (and the local Péclet number decreased), as expected for the energy norm setting, not robust with respect to the convection dominance. We then in Figure 5 plot the results for the 2.5 times longer final time $T = 1.5$. We find very similar results,

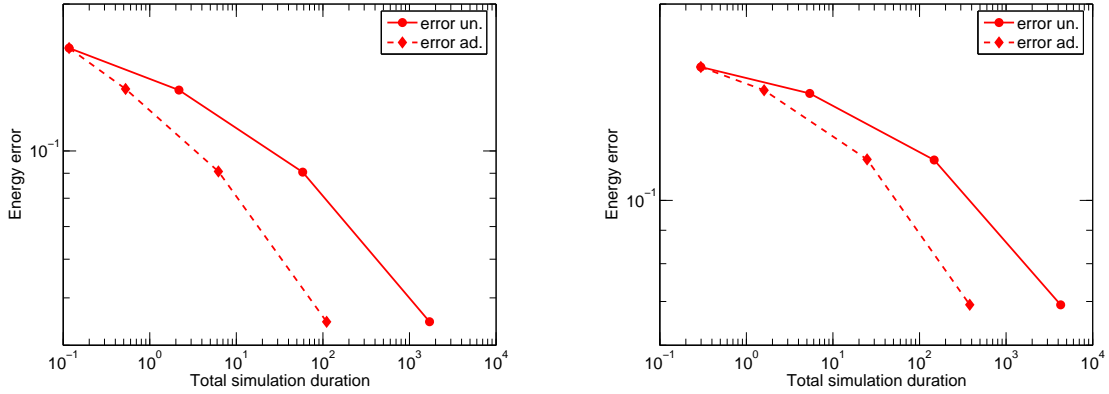


Figure 6: Errors in uniform/adaptive refinement as functions of the total CPU time, $\nu = 0.001$, $T = 0.6$ (left), $T = 1.5$ (right)

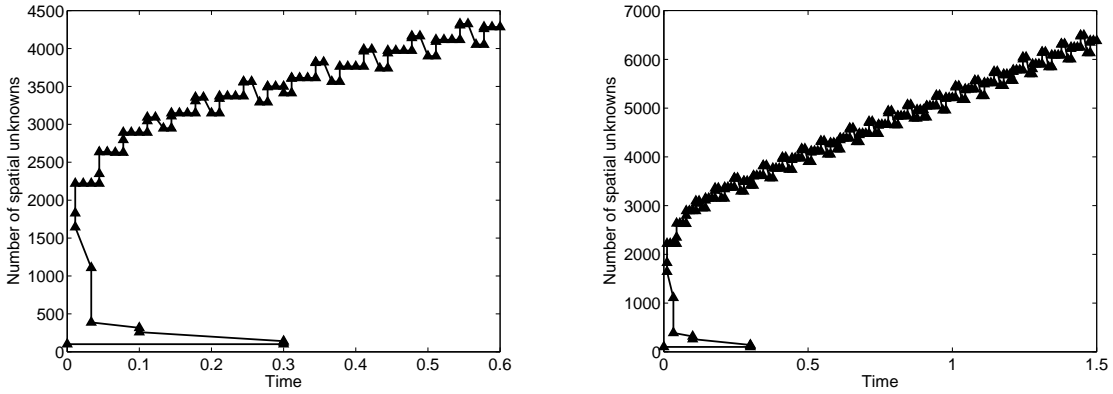


Figure 7: Evolution of the number of spatial unknowns as a function of the simulation time, $\nu = 0.001$, $T = 0.6$ (left) and $T = 1.5$ (right)

with in particular very similar effectivity indices. Our energy norm estimates thus seem to be independent of (robust with respect to) the final simulation time. In the uniform and adaptive cases, respectively, we find $\xi = 0.47$ and $\xi = 0.58$ for the experimental orders of convergence when $T = 1.5$.

Figure 6 then present the same results as the left parts of Figures 4 and 5, with this time the dependence of the errors in uniform and adaptive cases on the simulation duration. The results are, however, quite implementation/platform dependent, and we consider them as rather indicative only. In particular, the code TALISMAN [32], where our algorithm is implemented, is not optimized for the adaptive case yet. The computation in the uniform case is, on the other hand, slowed down by the fact that at each time step, the energy error contribution is computed, which we need in the present test setting. We finally, in Figure 7, illustrate another aspect of the performance of the adaptive algorithm of Section 6: we can see that from the original coarse time step $\tau_1 = 0.3$, the algorithm rapidly arrives at the minimal allowed time step of length $0.3/3^3$ (recall that $N_{\text{tm}} = 4$) while simultaneously increasing the number of space unknowns (located there where the spatial error is increased) from the original 100 to roughly 2200.

The left parts of Figures 4 and 5 also show the two components of η : the total diffusive and

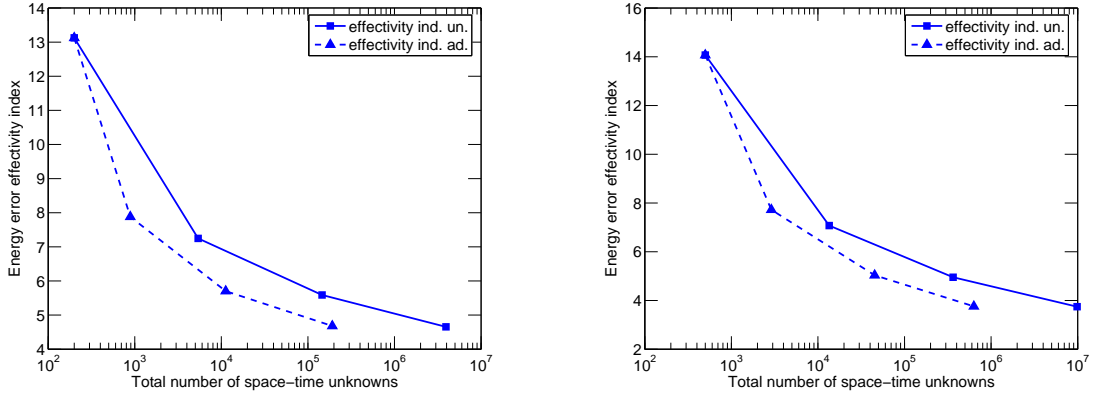


Figure 8: Effectivity indices for the estimators $\eta_{\text{DOQ},D}^n$ only, $\nu = 0.001$, $T = 0.6$ (left) and $T = 1.5$ (right)

convective flux estimator given by

$$\left\{ \sum_{n=1}^N \int_{t_{n-1}}^{t_n} \sum_{D \in \mathcal{D}_h^n} (\eta_{\text{DCF},D}^n(t))^2 dt \right\}^{\frac{1}{2}},$$

where $\eta_{\text{DCF},D}^n$ is given by (4.9), and the total data oscillation–quadrature estimator

$$\left\{ \sum_{n=1}^N \int_{t_{n-1}}^{t_n} \sum_{D \in \mathcal{D}_h^n} (\eta_{\text{DOQ},D}^n(t))^2 dt \right\}^{\frac{1}{2}},$$

where $\eta_{\text{DOQ},D}^n$ is given by (4.12). We remind that the residual estimators $\eta_{\text{R},D}^n$ given by (4.8) are all zero here thanks to the chosen construction of the diffusive and convective flux reconstructions $\boldsymbol{\theta}_h$ and \mathbf{w}_h . We can see that the data oscillation–quadrature estimators represent the dominant part of η . In the present case, these estimators only stem from the use of the mass lumping in the time evolution term; they would equal to zero if the discretization $\frac{u_D^n - \bar{u}_D^{n-1}}{\tau_n}$ of the temporal derivative in the scheme (3.1) was replaced by the term $(u_{h,\tau})_t$. Figure 8 shows the effectivity indices for the estimate given by the (constant-free) diffusive and convective flux estimators $\eta_{\text{DCF},D}^n$ (4.9) only. We can see that they are much closer to the optimal value of 1.

We next compare the uniform and adaptive refinement strategies visually, for $\nu = 0.001$ and $T = 0.6$. Figure 9 shows the approximate solution at the final time obtained in the adaptive case with $N_{\text{sp}} = N_{\text{tm}} = 2$ (left) and $N_{\text{sp}} = N_{\text{tm}} = 4$ (right). We can see that whereas in the first case, the numerical diffusion is extremely strong (notice that it only applies in the streamline direction by the definition of the local Péclet upstream weighting (3.7)), in the second one the approximate solution starts to capture the exact one rather well. Figure 10 then compares the uniform refinement strategy with the adaptive one. In its left part, the uniform refinement approximate solution at the final time with $N_{\text{sp}} = N_{\text{tm}} = 3$ is shown, whereas in its right part, we present its adaptive refinement counterpart for $N_{\text{sp}} = N_{\text{tm}} = 4$. The adaptive case gives clearly much better results, and this for roughly the same total number of space–time unknowns.

We finally focus on the diffusion-dominated case $\nu = 10$ (we consider $T = 1.5$). In this case, the adaptive refinement strategy does not lead to important improvements and hence we only present results for the uniform refinement. In Figure 11, the effectivity index is excellent as very close

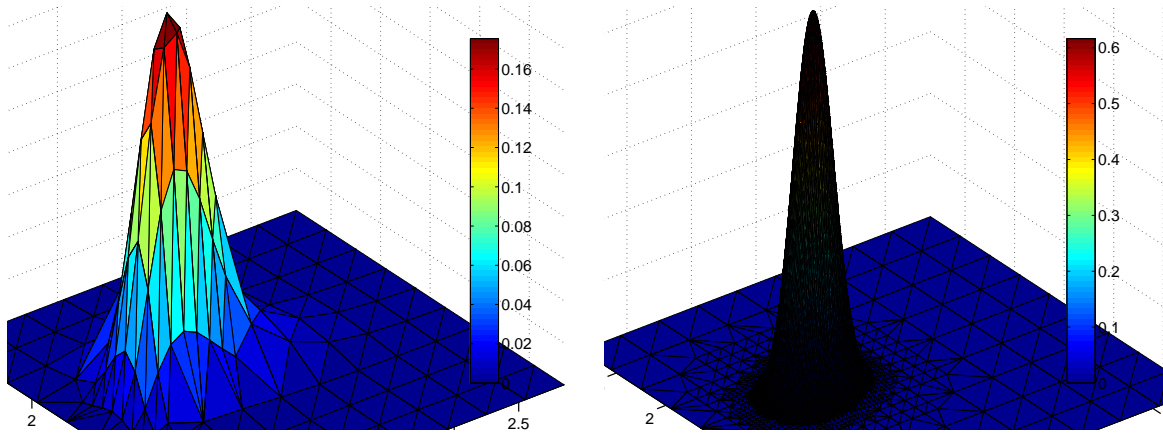


Figure 9: Adaptive refinement approximate solutions for $\nu = 0.001$, $T = 0.6$, and $N_{\text{sp}} = N_{\text{tm}} = 2$ (left) and $N_{\text{sp}} = N_{\text{tm}} = 4$ (right)

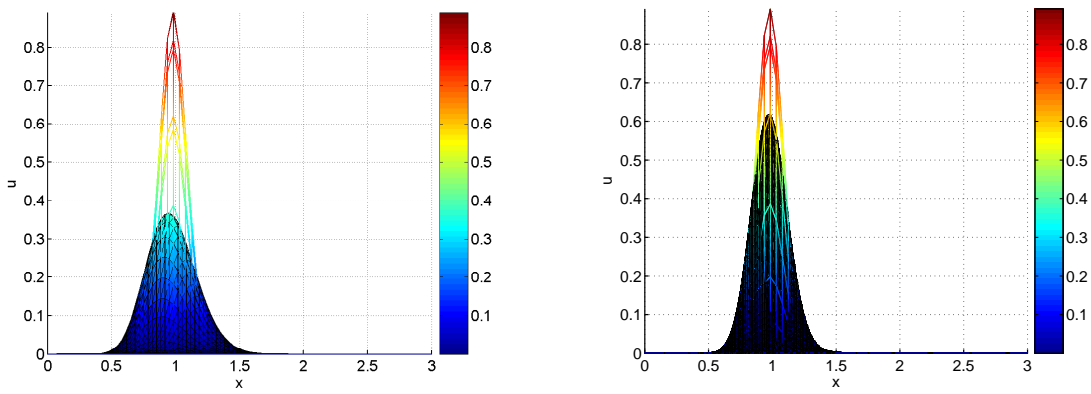


Figure 10: Uniform refinement approximate solution for $N_{\text{sp}} = N_{\text{tm}} = 3$ (left) and adaptive refinement approximate solution for $N_{\text{sp}} = N_{\text{tm}} = 4$ (right), $\nu = 0.001$ and $T = 0.6$

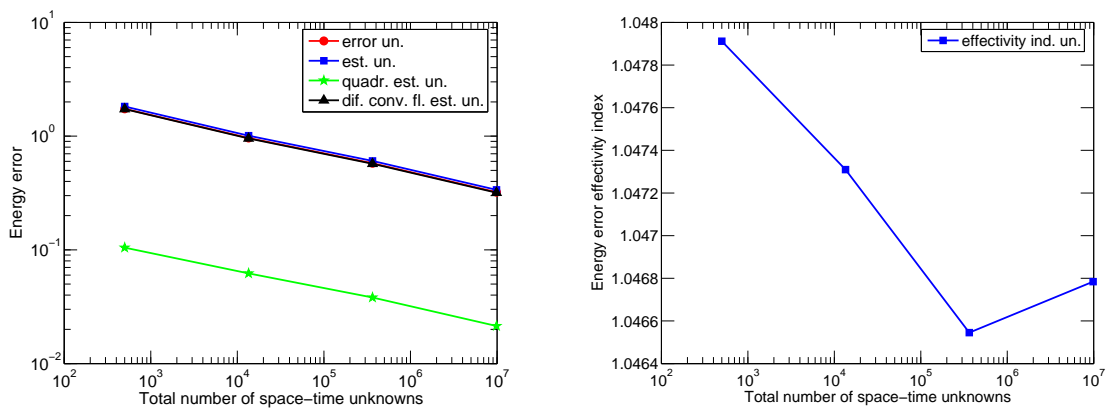


Figure 11: Estimated and actual energy errors (left) and corresponding effectivity indices (right), $\nu = 10$, $T = 1.5$

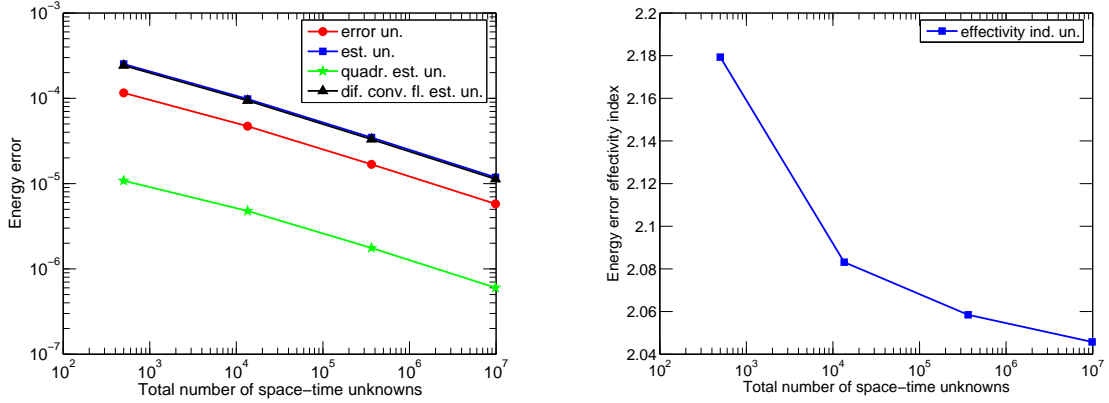


Figure 12: Estimated and actual energy errors (left) and corresponding effectivity indices (right), $\nu = 10$, $T = 1.5$, and $t_0 = 0.5$

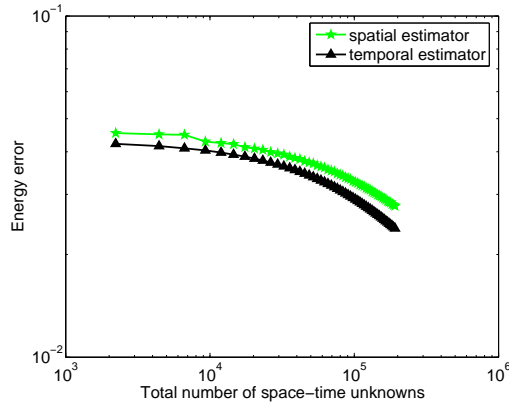


Figure 13: Spatial estimators η_{sp}^n and temporal estimators η_{tm}^n as a function of the number of space-time unknowns, $\nu = 0.001$, $T = 0.6$, $N_{\text{sp}} = N_{\text{tm}} = 4$

to the optimal value of one. This is probably caused by the fact that the exact solution almost instantaneously diffuses from the maximal value of 1 to the final maximal value of order 10^{-4} . Coincidentally, the experimental order of convergence $\xi = 0.53$ only. The solution presents much smoother behavior for the parameter $t_0 = 0.5$, in which case ξ takes the almost optimal value 0.97. We illustrate this case in Figure 12.

7.2 Equilibration of the spatial and temporal errors

One of the distinctive features of the algorithm of Section 6 is that it distinguishes the spatial and temporal parts of the error and tries to equilibrate them adaptively. We present in Figure 13 an illustration of the fact that this algorithm indeed succeeds in doing so: throughout the whole simulation for the diffusion parameter $\nu = 0.001$, final time $T = 0.6$, and the maximal allowed spatial and temporal refinements $N_{\text{sp}} = N_{\text{tm}} = 4$, the spatial estimators η_{sp}^n given by (4.14) and the temporal estimators η_{tm}^n given by (4.15) are approximately of the same size.

Figures 14 and 15 illustrate that such an equilibration is optimal: in Figure 14, we overrefine in time (we set $N_{\text{sp}} = 3$, $N_{\text{tm}} = 5$), whereas in Figure 15, we overrefine in space (we set $N_{\text{sp}} = 5$, $N_{\text{tm}} = 3$). In the left parts of these figures, we can see that the spatial and temporal estimators

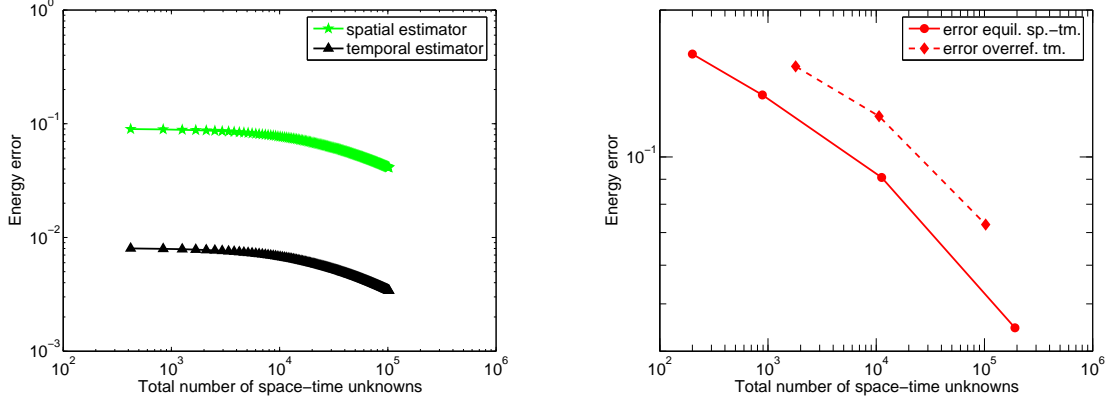


Figure 14: Spatial and temporal estimators for overrefinement in time (left) and comparison of the corresponding energy error with the equilibrated case (right), $\nu = 0.001$, $T = 0.6$

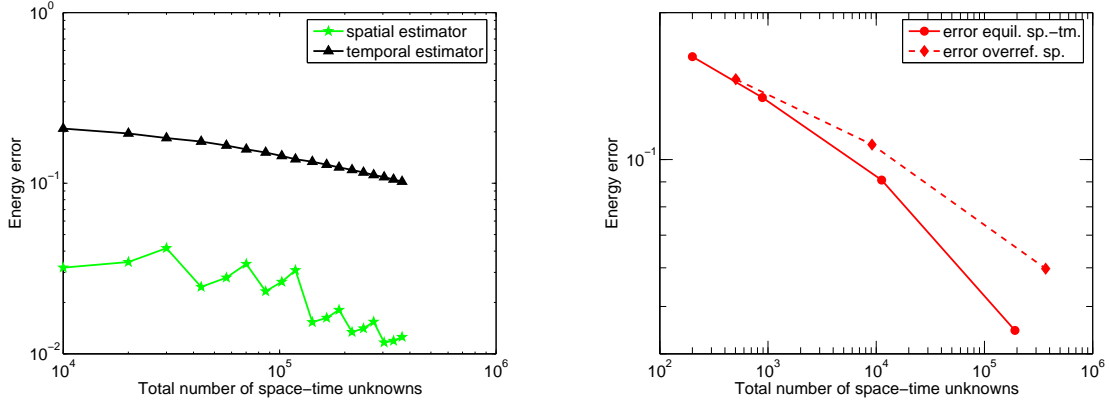


Figure 15: Spatial and temporal estimators for overrefinement in space (left) and comparison of the corresponding energy error with the equilibrated case (right), $\nu = 0.001$, $T = 0.6$

are now disequilibrated. More importantly, much worse precision for a given computational effort is now achieved in comparison with the equilibrated case, as we can see in the right parts of the Figures 14 and 15.

Remark that a key property is that both the spatial estimators η_{sp}^n and the temporal estimators η_{tm}^n are guaranteed (there is no unknown constant in either of them). This represents a conceptual difference with the classical residual-based estimators such as those of [21, 24, 25], where a spatial and a temporal estimator may also be defined, but where both of them feature an unknown constant. With a wrong choice of this unknown constant, one may easily overestimate or underestimate either the actual spatial or the actual temporal part of the error, leading to a situation like those in Figures 14 and 15. Thus, at least for the present numerical experiment, the suggested spatial and temporal estimators indeed control the error in space and time, respectively, and seem superior in this respect over the classical residual-based ones.

8 Conclusions

In Section 4 of this paper, we have derived a guaranteed a posteriori error estimate for transient linear convection-dominated convection–diffusion–reaction problems, discretized by vertex-centered finite-volume-type methods. This estimate is based on $\mathbf{H}(\operatorname{div}, \Omega)$ -conforming locally conservative reconstructions of both the diffusive and convective fluxes. It is particularly easy to calculate in the setting of the energy norm (2.3); herein, the principal diffusive and convective flux estimators $\eta_{\text{DCF}, D}^n$ given by (4.9) are constant-free. In the setting of the augmented norm (2.7), the derived estimate is robust with respect to all convection or reaction dominance and the final time. We have in this work particularly focused on the use of nonmatching grids, of upwinding, or of mass lumping; all these features are included in the definition of our combined finite volume–finite element scheme (3.1).

An important vocation of the present paper was the proposition and implementation of an adaptive algorithm, based on our a posteriori error estimates (cf. Section 6). This algorithm is proposed in the twofold objective of (a) guaranteeing that a user-given relative precision will be achieved at the end of the simulation and (b) ensuring that the calculation will be carried out as efficiently as possible. The second point is partly achieved by distinguishing the spatial and temporal parts of the error and by equilibrating them. The numerical experiments of Section 7 have confirmed that our spatial and temporal estimators indeed control the error in time and space. These experiments also showed that our estimates enable to predict very precisely the spatial error distribution. Consequently, using our adaptive algorithm, much better precision can be achieved for a given number of unknowns/given CPU time than with a uniform refinement. The effectivity index (overestimation factor) is rather increased in the energy norm setting in the convection-dominated regime. It, however, gets quite close to the optimal value of one with space and time mesh refinements or while increasing the influence of diffusion, thus ensuring optimal overall error control. In future works, we intend to extend the present methodology to nonlinear cases and/or to systems of partial differential equations, taking up the analysis in [8].

References

- [1] AMAZIANE, B., BERGAM, A., EL OSSMANI, M., AND MGHAZLI, Z. A posteriori estimators for vertex centred finite volume discretization of a convection-diffusion-reaction equation arising in flow in porous media. *Internat. J. Numer. Methods Fluids* 59, 3 (2009), 259–284.
- [2] ANGERMANN, L. An a posteriori estimation for the solution of elliptic boundary value problems by means of upwind FEM. *IMA J. Numer. Anal.* 12, 2 (1992), 201–215.
- [3] BEBENDORF, M. A note on the Poincaré inequality for convex domains. *Z. Anal. Anwendungen* 22, 4 (2003), 751–756.
- [4] BREZZI, F., AND FORTIN, M. *Mixed and hybrid finite element methods*, vol. 15 of *Springer Series in Computational Mathematics*. Springer-Verlag, New York, 1991.
- [5] CARSTENSEN, C., AND FUNKEN, S. A. Constants in Clément-interpolation error and residual based a posteriori error estimates in finite element methods. *East-West J. Numer. Math.* 8, 3 (2000), 153–175.
- [6] CARSTENSEN, C., LAZAROV, R., AND TOMOV, S. Explicit and averaging a posteriori error estimates for adaptive finite volume methods. *SIAM J. Numer. Anal.* 42, 6 (2005), 2496–2521.

- [7] CHEDDADI, I., FUČÍK, R., PRIETO, M. I., AND VOHRALÍK, M. Guaranteed and robust a posteriori error estimates for singularly perturbed reaction–diffusion problems. *M2AN Math. Model. Numer. Anal.* 43, 5 (2009), 867–888.
- [8] EL ALAOU, L., ERN, A., AND VOHRALÍK, M. Guaranteed and robust a posteriori error estimates and balancing discretization and linearization errors for monotone nonlinear problems. *Comput. Methods Appl. Mech. Engrg.* (2010). DOI 10.1016/j.cma.2010.03.024.
- [9] ERIKSSON, K., AND JOHNSON, C. Adaptive streamline diffusion finite element methods for stationary convection–diffusion problems. *Math. Comp.* 60, 201 (1993), 167–188, S1–S2.
- [10] ERN, A., STEPHANSEN, A. F., AND VOHRALÍK, M. Guaranteed and robust discontinuous Galerkin a posteriori error estimates for convection–diffusion–reaction problems. *J. Comput. Appl. Math.* 234, 1 (2010), 114–130.
- [11] ERN, A., AND VOHRALÍK, M. A posteriori error estimation based on potential and flux reconstruction for the heat equation. *SIAM J. Numer. Anal.* 48, 1 (2010), 198–223.
- [12] EYMARD, R., GALLOUËT, T., AND HERBIN, R. Finite volume methods. In *Handbook of Numerical Analysis, Vol. VII*. North-Holland, Amsterdam, 2000, pp. 713–1020.
- [13] EYMARD, R., HILHORST, D., AND VOHRALÍK, M. A combined finite volume–finite element scheme for the discretization of strongly nonlinear convection–diffusion–reaction problems on nonmatching grids. *Numer. Methods Partial Differential Equations* 26, 3 (2010), 612–646.
- [14] FEISTAUER, M., FELCMAN, J., LUKÁČOVÁ-MEDVID’OVÁ, M., AND WARNECKE, G. Error estimates for a combined finite volume–finite element method for nonlinear convection–diffusion problems. *SIAM J. Numer. Anal.* 36, 5 (1999), 1528–1548.
- [15] FELCMAN, J., AND KUBERA, P. An adaptive finite volume method for non-stationary problems. In *Finite volumes for complex applications V*. ISTE, London, 2008, pp. 407–414.
- [16] JU, L., WU, W., AND ZHAO, W. Adaptive finite volume methods for steady convection–diffusion equations with mesh optimization. *Discrete Contin. Dyn. Syst. Ser. B* 11, 3 (2009), 669–690.
- [17] LAZAROV, R., AND TOMOV, S. A posteriori error estimates for finite volume element approximations of convection–diffusion–reaction equations. *Comput. Geosci.* 6, 3-4 (2002), 483–503. Locally conservative numerical methods for flow in porous media.
- [18] NICAISE, S. A posteriori error estimations of some cell centered finite volume methods for diffusion–convection–reaction problems. *SIAM J. Numer. Anal.* 44, 3 (2006), 949–978.
- [19] OHLBERGER, M. A posteriori error estimates for vertex centered finite volume approximations of convection–diffusion–reaction equations. *M2AN Math. Model. Numer. Anal.* 35, 2 (2001), 355–387.
- [20] PAYNE, L. E., AND WEINBERGER, H. F. An optimal Poincaré inequality for convex domains. *Arch. Rational Mech. Anal.* 5 (1960), 286–292.
- [21] PICASSO, M. Adaptive finite elements for a linear parabolic problem. *Comput. Methods Appl. Mech. Engrg.* 167, 3-4 (1998), 223–237.

- [22] STEPHANSEN, A. F. *Méthodes de Galerkin discontinues et analyse d'erreur a posteriori pour les problèmes de diffusion hétérogène*. Ph.D. thesis, Ecole Nationale des Ponts et Chaussées, 2007.
- [23] VERFÜRTH, R. A posteriori error estimators for convection–diffusion equations. *Numer. Math.* 80, 4 (1998), 641–663.
- [24] VERFÜRTH, R. A posteriori error estimates for finite element discretizations of the heat equation. *Calcolo* 40, 3 (2003), 195–212.
- [25] VERFÜRTH, R. Robust a posteriori error estimates for nonstationary convection-diffusion equations. *SIAM J. Numer. Anal.* 43, 4 (2005), 1783–1802.
- [26] VERFÜRTH, R. Robust a posteriori error estimates for stationary convection-diffusion equations. *SIAM J. Numer. Anal.* 43, 4 (2005), 1766–1782.
- [27] VERFÜRTH, R. A note on constant-free a posteriori error estimates. *SIAM J. Numer. Anal.* 47, 4 (2009), 3180–3194.
- [28] VOHRALÍK, M. On the discrete Poincaré–Friedrichs inequalities for nonconforming approximations of the Sobolev space H^1 . *Numer. Funct. Anal. Optim.* 26, 7–8 (2005), 925–952.
- [29] VOHRALÍK, M. A posteriori error estimation in the conforming finite element method based on its local conservativity and using local minimization. *C. R. Math. Acad. Sci. Paris* 346, 11–12 (2008), 687–690.
- [30] VOHRALÍK, M. Residual flux-based a posteriori error estimates for finite volume and related locally conservative methods. *Numer. Math.* 111, 1 (2008), 121–158.
- [31] VOHRALÍK, M. Guaranteed and fully robust a posteriori error estimates for conforming discretizations of diffusion problems with discontinuous coefficients. *J. Sci. Comput.* (2010). Accepted for publication.
- [32] VOHRALÍK, M., AND RAMAROSY, N. Talisman, a finite volume–finite element tool for numerical simulation of subsurface flow and contaminant transport with a posteriori error control and adaptive mesh refinement. Presentation and User guide. Tech. rep., HydroExpert, 53 rue Charles Frérot, 94 250 Gentilly, France, www.hydroexpert.com, 2007.